arXiv:2603.09790v1 [math.NA] 10 Mar 2026

# Scalable s-step Preconditioned Conjugate Gradient with Chebyshev Basis and Gauss–Seidel Gram Solve*

Pasqua D'Ambra† Massimo Bernaschi‡ Mauro G. Carrozzo‡
Stephen Thomas§

March 11, 2026

**Abstract**

We present a variant of the $s$-step Preconditioned Conjugate Gradient (PCG) method that combines a Chebyshev-stabilized Krylov basis with a Forward Gauss–Seidel (FGS) iteration for the solution of the reduced Gram systems. In $s$-step Conjugate Gradient, multiple search directions are generated per outer iteration, reducing global synchronization costs but requiring the solution of small dense Gram systems whose conditioning is critical for stability.

We analyze the structure of the Chebyshev Gram matrix and show that its moment-based representation is associated with favorable conditioning properties for moderate step sizes. Building on inexact Krylov theory and on the classical equivalence between FGS and Modified Gram–Schmidt (MGS), we provide a structural analysis and theoretical rationale supporting the use of a small number of FGS sweeps, while preserving the convergence behavior observed in practical regimes.

Large-scale experiments on modern NVIDIA GPU architectures demonstrate that the proposed Chebyshev–stabilized, Gauss–Seidel–enhanced $s$-step PCG achieves convergence comparable to classical CG while reducing synchronization overhead, making it a stable and scalable alternative for current and next-generation accelerator systems.

## 1 Introduction

We consider the numerical solution of large, sparse, symmetric positive–definite (SPD) linear systems

$$Ax = b, \qquad A \in \mathbb{R}^{n\times n}, \quad x, b \in \mathbb{R}^n.$$

*This work was partially supported by: Spoke 6 "Multiscale Modelling & Engineering Applications" of the Italian Research Center on High-Performance Computing, Big Data and Quantum Computing (ICSC) funded by MUR-NextGenerationEU (NGEU); the "Energy Oriented Center of Excellence (EoCoE III): Fostering the European Energy Transition with Exascale" EuroHPC Project N. 101144014, funded by European Commission (EC).

†Institute for Applied Computing "Mauro Picone", National Research Council of Italy, Via Pietro Castellino, 111, Naples 80131, Italy. (pasqua.dambra@cnr.it)

‡Institute for Applied Computing "Mauro Picone", National Research Council of Italy, Via dei Taurini, 19, Rome 00185, Italy. (massimo.bernaschi@cnr.it,maurogiovanni.carrozzo@cnr.it)

§Department of Computer Science and Engineering, Lehigh University, 27 Memorial Drive West, Bethlehem, PA 18015, USA (sjt223@lehigh.edu)

Such systems arise ubiquitously in scientific and engineering applications including discretized partial differential equations, optimization, and data analysis. For large-scale problems, direct solvers are often impractical due to their memory footprint and superlinear complexity, making iterative methods essential. Among them, the Preconditioned Conjugate Gradient (PCG) method is the standard algorithm for SPD systems. Let $M$ be an SPD preconditioner and define the preconditioned operator

$$\mathcal{A} := M^{-1}A.$$

Given an initial guess $x_0$ and residual $r_0 = b - Ax_0$, PCG builds approximations $x_m$ in the preconditioned Krylov subspaces

$$\mathcal{K}_m(\mathcal{A}, M^{-1}r_0) = \operatorname{span}\{\, M^{-1}r_0,\ \mathcal{A}M^{-1}r_0,\ \ldots,\ \mathcal{A}^{m-1}M^{-1}r_0 \,\}.$$

The convergence of PCG depends directly on the spectrum of $\mathcal{A}$ and thus on the quality of the preconditioner. The choice of the preconditioner is therefore a critical design aspect, as it strongly affects both the convergence rate and the overall computational cost of the method. As a consequence, a significant amount of research has been devoted to the development of preconditioners that are both effective and scalable on modern high-performance computing architectures. In this work, however, we do not address the design of the preconditioner itself; instead, we focus on the intrinsic limitations of the PCG solver, which persist even in the presence of highly optimized preconditioners and stem from its algorithmic structure.

In particular, PCG relies on two additional performance-critical computational kernels: the sparse matrix–vector product (SpMV) and the computation of inner product (dot). SpMV is inherently memory-bandwidth bound and requires communication to exchange boundary data among neighboring processes, with a communication cost that depends on the sparsity pattern of the matrix and the underlying data partitioning. Importantly, this communication is typically local and structured, and several SpMV implementations have been shown to effectively overlap communication with computation, thereby mitigating its impact on scalability. In contrast, the computation of inner products entails global reduction operations, which impose global synchronization and introduce communication latencies that cannot be hidden, often emerging as the primary scalability bottleneck on massively parallel systems. These considerations motivate the development of Communication-Avoiding (CA) Krylov subspace methods, and in particular $s$-step formulations, which trade additional local computation for a significant reduction in global synchronization, thereby improving strong scalability on modern HPC architectures.

In $s$–step PCG [7, 8], the information from $s$ consecutive Krylov iterations is aggregated into a single block. A raw block Krylov basis is first constructed as

$$U = [\, u_0,\ \mathcal{A}u_0,\ \ldots,\ \mathcal{A}^{s-1}u_0 \,],$$

and the corresponding block of $A$-conjugate directions is obtained from a reduced Gram system involving $U$ and the previously computed search directions.

A well-known difficulty of this monomial construction is numerical instability: the vectors $\mathcal{A}^j u_0$ rapidly lose linear independence as $j$ increases, causing the Gram matrix in the $A$-inner product, $W = U^\top AU$, to become severely ill-conditioned. To mitigate this effect, one may replace the monomial basis with a scaled Chebyshev basis,

$$u_j = T_j(\mathcal{A})\, u_0, \qquad j = 0, \ldots, s-1,$$

where $T_j$ denotes the $j$-th Chebyshev polynomial of the first kind mapped to the spectrum of $\mathcal{A}$. This yields a significantly better-conditioned block basis for the $s$–step PCG framework. As shown by Philippe and Reichel [20], this construction produces Gram matrices whose condition number grows only quadratically with $s$, in contrast to the exponential growth associated with monomial bases.

Two reduced Gram systems must be solved at every outer iteration. To solve them efficiently, we use a small, fixed number of Forward Gauss–Seidel (FGS) iterations. This choice is supported by the classical equivalence between one FGS sweep on a Gram system and one Modified Gram–Schmidt pass in the corresponding inner product, which provides a stability rationale for the proposed inexact solve. An earlier version of the FGS–based Gram-solver analysis appeared in [25]. The present work extends it with a structural moment-based analysis of Chebyshev Gram matrices, a performance model for multi–GPU architectures, and a large-scale experimental evaluation within the BootCMatchGX software framework.

The main contributions of this work can be summarized as follows.

- We propose a scalable $s$-step PCG formulation that combines a Chebyshev–stabilized Krylov basis with FGS iterations for the reduced Gram solves. The formulation targets GPU architectures by reducing global synchronization points and reformulating low arithmetic-intensity BLAS-1 operations as block BLAS-3 kernels (matrix–matrix products), enabling efficient utilization of GPU throughput.

- We provide a structural analysis of the Chebyshev Gram matrix, showing that its moment-based representation explains its favorable conditioning properties for moderate step sizes and clarifies the role of spectral regularity and preconditioning in practice.

- Building on inexact Krylov theory and on the classical equivalence between FGS and MGS, we identify practically motivated conditions under which the inexact Gram solve is consistent with the convergence behavior of the outer $s$-step PCG iteration, supported by numerical evidence; a fully rigorous sufficient condition would require a lower bound on $\sigma_{\min}(U)$, the minimum singular value of $U$, which is not established here.

- We develop a performance model that quantifies the trade-off between reduced global synchronization and increased local computation, and we validate the analysis through strong and weak scaling experiments on modern multi-GPU supercomputers.

- To the best of our knowledge, this is the first available fully distributed multi-GPU implementation and large-scale experimental evaluation of preconditioned $s$-step CG. The method is implemented within the open-source BootCMatchGX framework[1], enabling reproducibility and further research on scalable communication-reducing Krylov methods.

The remainder of the paper is organized as follows. Section 2 introduces the $s$-step PCG method with Chebyshev Krylov basis. Section 3 analyzes the inexact solution of the Chebyshev Gram systems and discusses its stability and convergence implications.

[1] https://github.com/bootcmatch/BootCMatchGX

Section 4 summarizes details on our practical implementation of the method and presents the performance model. Section 5 reviews related work. Section 6 reports numerical results on large-scale GPU platforms, and Section 7 concludes the paper with final remarks and future work.

## 2 The $s$-step PCG method with Chebyshev Krylov basis

The $s$-step preconditioned Conjugate Gradient (PCG-S) method considered in this work is summarized in Algorithm 1. Given an initial guess $x^{(0)}$ and residual $r^{(0)} = b - Ax^{(0)}$, the PCG-S method proceeds by grouping $s$ consecutive Krylov iterations into a single outer iteration. At each outer iteration $k$, a block Krylov subspace of dimension $s$ is constructed using a Chebyshev polynomial basis associated with the current residual $r^{(k)}$.

Let $\lambda_{\min}$ and $\lambda_{\max}$ denote the minimum and maximum eigenvalues of $A$, respectively, and let

$$\widehat{A} = \frac{2A - (\lambda_{\max} + \lambda_{\min})I}{\lambda_{\max} - \lambda_{\min}}$$

denote the shifted and scaled operator mapping the spectrum of $A$ to $[-1, 1]$.

The Chebyshev Krylov basis is defined as

$$Z_k = \left[z_1^{(k)}, \ldots, z_s^{(k)}\right], \qquad z_j^{(k)} = M^{-1} T_{j-1}(\widehat{A}) r^{(k)},$$

where $T_j$ is the Chebyshev polynomial of degree $j$ of the first kind. The construction of $Z_k$, together with the augmented product matrix

$$P_k = \left[r^{(k)},\ Az_1^{(k)},\ \ldots,\ Az_s^{(k)}\right] \in \mathbb{R}^{n \times (s+1)},$$

whose first column carries the current residual and whose remaining columns carry the products $AZ_k$, is obtained by means of the so-called Matrix Power Kernel (MPK), as described in Algorithm 2. The parameters $\alpha$, $\sigma$, and $\gamma$ appearing in Algorithm 2 arise directly from the three–term recurrence relation satisfied by Chebyshev polynomials:

$$T_{j+1}(x) = 2x\, T_j(x) - T_{j-1}(x).$$

After spectral shifting and scaling, this recurrence translates into the vector relation

$$z_{j+1} = M^{-1}(2\alpha A z_j - 2\sigma z_j - \gamma z_{j-1}),$$

with parameters given by

$$\alpha = \frac{2}{\lambda_{\max} - \lambda_{\min}}, \qquad \sigma = \frac{\lambda_{\max} + \lambda_{\min}}{\lambda_{\max} - \lambda_{\min}}, \qquad \gamma = 1.$$

The block of $A$-conjugate search directions is denoted by $Q_k \in \mathbb{R}^{n \times s}$. The approximate solution is updated as

$$x^{(k+1)} = x^{(k)} + Q_k \alpha_k,$$

where the coefficient vector $\alpha_k \in \mathbb{R}^s$ is obtained by solving the reduced Gram system, corresponding to the normal equations in the $A$-inner product and ensuring minimal error in the $A$-norm:

$$W_k \alpha_k = m_k, \qquad W_k := Q_k^\top A Q_k, \qquad m_k := Q_k^\top r^{(k)}.$$

The residual is then updated according to

$$r^{(k+1)} = r^{(k)} - AQ_k\alpha_k.$$

To enforce $A$-conjugacy between the newly generated Chebyshev basis $Z_{k+1}$ and the previously computed search directions, a second reduced Gram system with multiple right-hand sides is formed, whose solution yields the block coefficient matrix $\beta_k \in \mathbb{R}^{s\times s}$. Specifically, requiring $(Q_{k+1})^\top AQ_k = 0$ with $Q_{k+1} = Z_{k+1} + Q_k\beta_k$ gives

$$W_k\beta_k = -Q_k^\top AZ_{k+1},$$

whose right-hand side is assembled as $b_2 \leftarrow -Q^\top AQ_{\text{new}}$ at line 12 of Algorithm 1.

The new search directions are obtained via the block update

$$Q_{k+1} = Z_{k+1} + Q_k\beta_k, \qquad AQ_{k+1} = AZ_{k+1} + AQ_k\beta_k,$$

which corresponds to line 15 of Algorithm 1. This update is the direct block analogue of the classical CG recurrence and preserves $A$-conjugacy while avoiding additional applications of the operator $A$.

This block formulation also has important computational implications. In classical CG, most algebraic operations consist of Level 1 Basic Linear Algebra Subprograms (BLAS-1) vector kernels (dot products and axpy updates), which have low arithmetic intensity and limited efficiency on modern accelerators. In contrast, the $s$-step formulation naturally aggregates vectors into blocks, so that these operations can be reformulated as matrix–vector and matrix–matrix products involving the block bases $Z_k$, $Q_k$, and $AQ_k$. As a result, many BLAS-1 operations are replaced by BLAS-2/3 kernels (e.g., GEMV and GEMM), increasing arithmetic intensity and enabling more efficient utilization of GPU architectures.

**Algorithm 1** Preconditioned s-step Conjugate Gradient (PCG-S) Algorithm

**Require:** $A \in \mathbb{R}^{n\times n}$, $b \in \mathbb{R}^n$, $x^{(0)}$, preconditioner $M$, step size $s$, tolerance $\tau$, maximum iterations $k_{\max}$

**Ensure:** Approximate solution $x^{(k)}$

1: $r^{(0)} \leftarrow b - Ax^{(0)}$
2: $[Z, P] \leftarrow \text{MPK}(A, r^{(0)}, s, M^{-1}, \text{basis_info})$
3: $Q \leftarrow Z, \quad AQ \leftarrow P(:, 2:\text{end})$
4: **for** $k = 0, 1, \ldots, k_{\max} - 1$ **do**
5: $\quad W \leftarrow Q^\top AQ, \quad b_1 \leftarrow Q^\top P(:, 1)$
6: $\quad \alpha \leftarrow \text{FGS}(W, b_1, iter_{GS})$
7: $\quad x^{(k+1)} \leftarrow x^{(k)} + Q\alpha$
8: $\quad r^{(k+1)} \leftarrow r^{(k)} - AQ\alpha$
9: $\quad$ **if** $\|r^{(k+1)}\| \le \tau\|b\|$ **then stop**
10: $\quad$ **end if**
11: $\quad [Z, P] \leftarrow \text{MPK}(A, r^{(k+1)}, s, M^{-1}, \text{basis_info})$
12: $\quad AQ_{\text{new}} \leftarrow P(:, 2:\text{end})$
13: $\quad b_2 \leftarrow -Q^\top AQ_{\text{new}}$
14: $\quad \beta \leftarrow \text{FGS}(W, b_2, iter_{GS})$
15: $\quad Q \leftarrow Z + Q\beta, \quad AQ \leftarrow AQ_{\text{new}} + AQ\beta$
16: **end for**

**Algorithm 2** MPK for Chebyshev basis

**Require:** $A \in \mathbb{R}^{n\times n}$, $r \in \mathbb{R}^n$, step size $s \geq 1$, preconditioner $M$, basis parameters $(\alpha, \sigma, \gamma)$

**Ensure:** Matrices $Z = [z_1, \ldots, z_s]$, $P = [p_1, \ldots, p_s, p_{s+1}]$

```
p_1 ← r;    zp_1 ← p_1;    z_1 ← M^{-1} zp_1
if s > 1 then
    p_2 ← A z_1
    zp_2 ← α p_2 − σ zp_1
    z_2 ← M^{-1} zp_2
    if s > 2 then
        for q = 2 to s − 1 do
            p_{q+1} ← A z_q
            zp_{q+1} ← 2α p_{q+1} − 2σ zp_q − γ zp_{q−1}
            z_{q+1} ← M^{-1} zp_{q+1}
        end for
    end if
end if
p_{s+1} ← A z_s
return Z = [z_1, ..., z_s],   P = [p_1, ..., p_s, p_{s+1}]
```

In the following, we analyze the use of a small number of FGS iterations (function FGS at lines 6 and 14 of Algorithm 1) to approximate the reduced Gram solves arising in PCG-S, and identify conditions under which the resulting inexact inner solve remains compatible with the convergence of the outer iteration.

# 3 Iterated Gauss–Seidel Solution of the Chebyshev Gram System

According to inexact Krylov theory [30, 2], outer convergence is preserved provided that the perturbations introduced at each iteration remain sufficiently small relative to the current residual. A practical working criterion is that the approximate Gram solution satisfy the relative residual bound

$$\|m_k - W_k\alpha_k\| \;\leq\; \delta_k \, \|m_k\|, \tag{1}$$

with $\delta_k$ appropriately controlled; the connection to the rigorous perturbation bound of inexact Krylov theory is discussed in Remark 1 below.

Under a uniform bound $\delta_k \leq \delta$, the accumulated perturbation remains bounded over $N_{\text{outer}}$ iterations. In particular, a sufficient practical condition is that

$$N_{\text{outer}}\, \delta \lesssim 1, \tag{2}$$

so that the cumulative effect of the inexact solves does not dominate the convergence mechanism.

**Remark 1.** *We emphasize that condition (1) represents a practical tolerance for the inner Gram solve, while condition (2) should be interpreted as a heuristic sufficient condition rather than as a rigorously derived bound. A fully rigorous inexact Krylov analysis*

*(see [30, 2]) would control the perturbation relative to $\|r_k\|$ rather than $\|m_k\|$. Since $m_k = Q_k^T r_k$, relating these quantities requires a lower bound on $\sigma_{\min}(Q_k)$. Such a bound can in principle be obtained from the orthogonality properties of the block basis, but we do not pursue a formal derivation here. Instead, the condition $N_{\text{outer}}\delta \lesssim 1$ is used as a practical guideline for selecting the inner accuracy. Its suitability in the present context is supported by the numerical experiments reported in Sections 3.3 and 6.*

**Remark 2.** *Throughout this section, the outer iteration index $k$ is omitted for notational simplicity. The analysis is carried out for the Gram system defining $\alpha_k$ and extends directly to the Gram system with multiple right-hand sides defining $\beta_k$.*

## 3.1 Forward Gauss–Seidel iteration

The FGS iteration for the system $W\alpha = m$ with splitting $W = I + L + L^\top$ computes

$$(I + L)\,\alpha^{(\nu+1)} = m - L^\top \alpha^{(\nu)}, \tag{3}$$

which is equivalent to

$$\alpha^{(\nu+1)} = (I + L)^{-1}(m - L^\top \alpha^{(\nu)}) = (I + L)^{-1}m - (I + L)^{-1}L^\top \alpha^{(\nu)}. \tag{4}$$

The iteration matrix is $G = -(I + L)^{-1}L^\top$.

**Proposition 1** (Residual after $\nu$ FGS sweeps)**.** *Let $\alpha^{(0)} = 0$ and let $\alpha^{(\nu)}$ be obtained after $\nu$ forward Gauss–Seidel sweeps on $W\alpha = m$ with $W = I + L + L^\top$. Then the residual satisfies*

$$r^{(\nu)} := m - W\alpha^{(\nu)} = (-1)^\nu (L^\top (I + L)^{-1})^\nu m. \tag{5}$$

*Consequently,*

$$\|r^{(\nu)}\| \le \|L^\top (I + L)^{-1}\|^\nu \|m\|. \tag{6}$$

*Proof.* The proof proceeds by induction. For $\nu = 1$, the FGS iteration with $\alpha^{(0)} = 0$ gives $(I + L)\alpha^{(1)} = m$, so $\alpha^{(1)} = (I + L)^{-1}m$. The residual is

$$\begin{aligned} r^{(1)} &= m - W\alpha^{(1)} = m - (I + L + L^\top)(I + L)^{-1}m \\ &= m - m - L^\top (I + L)^{-1}m = -L^\top (I + L)^{-1}m, \end{aligned}$$

which confirms (5) for $\nu = 1$.

Assume the formula holds for $\nu$. From the FGS update (3),

$$(I + L)\,\alpha^{(\nu+1)} = m - L^\top \alpha^{(\nu)},$$

so, using $(I + L + L^\top)(I + L)^{-1} = I + L^\top (I + L)^{-1}$,

$$\begin{aligned} r^{(\nu+1)} &= m - W\alpha^{(\nu+1)} \\ &= m - (I + L + L^\top)(I + L)^{-1}(m - L^\top \alpha^{(\nu)}) \\ &= -L^\top (I + L)^{-1}\big(m - (I + L + L^\top)\alpha^{(\nu)}\big) \\ &= -L^\top (I + L)^{-1}\, r^{(\nu)}. \end{aligned}$$

By the inductive hypothesis, $r^{(\nu)} = (-1)^\nu (L^\top (I + L)^{-1})^\nu m$, giving

$$r^{(\nu+1)} = (-1)^{\nu+1}(L^\top (I + L)^{-1})^{\nu+1} m,$$

completing the induction. The bound (6) follows from submultiplicativity of the norm. □

**Corollary 1** (Asymptotic residual reduction rate)**.** *Let $\varrho := \varrho\big(L^\top (I+L)^{-1}\big)$ denote the spectral radius of the residual iteration matrix. Then for any $\varepsilon > 0$ there exists a constant $C = C(\varepsilon, W) > 0$, independent of $\nu$, such that*

$$\frac{\|r^{(\nu)}\|_2}{\|m\|_2} \;\le\; C\,(\varrho+\varepsilon)^\nu, \qquad \nu \ge 1. \tag{7}$$

*In particular, the FGS iteration converges if and only if $\varrho < 1$, and the asymptotic rate satisfies*

$$\limsup_{\nu\to\infty} \|r^{(\nu)}\|_2^{1/\nu} \;=\; \varrho\big(L^\top (I+L)^{-1}\big)\,. \tag{8}$$

**Remark 3.** *The convergence factor $\varrho$ is governed by the strictly triangular part $L$, whose magnitude depends on the polynomial basis used to construct the Krylov block. We show in the following subsections that Chebyshev bases control the size of $L$, ensuring $\varrho < 1$ for moderately large step sizes $s$.*

### 3.1.1 Structure of Chebyshev Gram Matrices

The Chebyshev basis employs the shifted-scaled Chebyshev polynomials $\widetilde{T}_j(A) = T_j(\widehat{A})$ where $\widehat{A} = (2A - (\lambda_{\max} + \lambda_{\min})I)/(\lambda_{\max} - \lambda_{\min})$ maps the spectrum of $A$ to $[-1, 1]$. The block Krylov basis is

$$S_{s+1} := \big[T_0(\widehat{A})r_0,\; T_1(\widehat{A})r_0,\; \ldots,\; T_s(\widehat{A})r_0\big].$$

Let $A = V\Lambda V^\top$ be the eigendecomposition with eigenvalues $\lambda_1 \le \cdots \le \lambda_n$ and let $c = V^\top r_0$ so that $c_\ell = q_\ell^\top r_0$. Define the transformed eigenvalues $\hat{\lambda}_\ell = (2\lambda_\ell - \lambda_{\max} - \lambda_{\min})/(\lambda_{\max} - \lambda_{\min}) \in [-1, 1]$.

The Gram matrix $W = S_{s+1}^\top S_{s+1}$ (using the standard inner product; the $A$-inner product case is analogous) has entries

$$W_{ij} = \sum_{\ell=1}^{n} |c_\ell|^2 T_{i-1}(\hat{\lambda}_\ell) T_{j-1}(\hat{\lambda}_\ell). \tag{9}$$

**Lemma 1** (Chebyshev product formula)**.** *For any $x \in [-1, 1]$,*

$$T_m(x)T_n(x) = \frac{1}{2}\big(T_{m+n}(x) + T_{|m-n|}(x)\big). \tag{10}$$

Applying (10) to (9) gives:

**Theorem 1** (Chebyshev Gram matrix structure)**.** *The Chebyshev Gram matrix has entries*

$$W_{ij} = \frac{1}{2}\big(\mu_{i+j-2} + \mu_{|i-j|}\big), \tag{11}$$

*where $\mu_p = \sum_{\ell=1}^{n} |c_\ell|^2 T_p(\hat{\lambda}_\ell)$ are the Chebyshev moments of the spectral measure induced by $(A, r_0)$.*

*Proof.* Substituting (10) into (9):

$$\begin{aligned} W_{ij} &= \sum_{\ell=1}^{n} |c_\ell|^2 T_{i-1}(\hat{\lambda}_\ell) T_{j-1}(\hat{\lambda}_\ell) \\ &= \sum_{\ell=1}^{n} |c_\ell|^2 \cdot \frac{1}{2}\big(T_{i+j-2}(\hat{\lambda}_\ell) + T_{|i-j|}(\hat{\lambda}_\ell)\big) \\ &= \frac{1}{2}\big(\mu_{i+j-2} + \mu_{|i-j|}\big). \end{aligned}$$

□

**Corollary 2** (Diagonal entries)**.** *$W_{ii} = \frac{1}{2}\big(\mu_0 + \mu_{2i-2}\big)$, with $\mu_0 = \sum_{\ell=1}^{n} |c_\ell|^2 = \|r_0\|^2$.*

The off-diagonal structure of $W$ is governed by the decay of Chebyshev moments $\mu_p$ as $p$ increases.

**Theorem 2** (Chebyshev moment bounds and decay under regularity)**.** *Let $\hat{\lambda}_\ell \in [-1, 1]$ and let*

$$\mu_p := \sum_{\ell=1}^{n} |c_\ell|^2 \, T_p(\hat{\lambda}_\ell), \qquad p \geq 0,$$

*where $T_p$ denotes the Chebyshev polynomial of the first kind. Define the normalized weights*

$$w_\ell := \frac{|c_\ell|^2}{\sum_{m=1}^{n} |c_m|^2}, \qquad \sum_{\ell=1}^{n} w_\ell = 1,$$

*and the normalized moments*

$$\tilde{\mu}_p := \sum_{\ell=1}^{n} w_\ell \, T_p(\hat{\lambda}_\ell), \qquad \textit{so that} \qquad \mu_p = \|r_0\|^2 \, \tilde{\mu}_p, \quad \tilde{\mu}_0 = 1.$$

*Then:*

1. ***Uniform bound.*** *For all $p \geq 0$,*

$$|\mu_p| \leq \|r_0\|^2 \qquad \textit{and} \qquad |\tilde{\mu}_p| \leq 1.$$

2. ***Decay for absolutely continuous spectral measures.*** *We note that Parts* (2) *and* (3) *apply to the* limit measure *$\mu$ to which the induced discrete spectral measures converge weakly as $n \to \infty$, the standard regime for PDE operators under mesh refinement. For any fixed finite $n$ the induced measure is purely discrete and Part* (1) *is the only available bound; see the remark 4.*

   *Assume that the limit measure is absolutely continuous with normalized density $\varphi \in L^1([-1, 1])$, i.e.,*

$$\tilde{\mu}_p = \int_{-1}^{1} T_p(t) \, \varphi(t) \, dt, \qquad \varphi \geq 0, \quad \int_{-1}^{1} \varphi(t) \, dt = 1.$$

   *Then $\tilde{\mu}_p \to 0$ as $p \to \infty$, and hence $\mu_p \to 0$. For finite $n$ the discrete moments $\tilde{\mu}_p^{(n)}$ converge to $\tilde{\mu}_p$ as $n \to \infty$ and therefore satisfy the same decay bound for all sufficiently large $n$.*

3. ***Algebraic decay under smoothness.*** *Assume in addition that the function*

$$h(\theta) := \varphi(\cos\theta) \, \sin\theta, \qquad \theta \in [0, \pi],$$

   *belongs to $W^{q,1}(0, \pi)$ for some integer $q \geq 1$ (i.e., $h$ is absolutely continuous up to order $q - 1$ and $h^{(q)} \in L^1(0, \pi)$). Then there exists a constant $C_q > 0$ such that*

$$|\tilde{\mu}_p| \leq \frac{C_q}{p^q}, \qquad p \geq 1,$$

   *and therefore $|\mu_p| \leq \|r_0\|^2 \, C_q \, p^{-q}$. The constant $C_q = \|h^{(q)}\|_{L^1(0,\pi)}$ depends on the spectral density of the limit measure but not on $n$; the bound is therefore uniform in $n$.*

*Proof.* *(1)* Since $|T_p(t)| \le 1$ for all $t \in [-1,1]$ and $p \ge 0$,

$$|\mu_p| = \left| \sum_{\ell=1}^{n} |c_\ell|^2 \, T_p(\hat{\lambda}_\ell) \right| \le \sum_{\ell=1}^{n} |c_\ell|^2 \, |T_p(\hat{\lambda}_\ell)| \le \sum_{\ell=1}^{n} |c_\ell|^2 = \|r_0\|^2.$$

Dividing by $\|r_0\|^2$ yields $|\tilde{\mu}_p| \le 1$.

*(2)* Using the standard identity $T_p(\cos\theta) = \cos(p\theta)$ and the substitution $t = \cos\theta$ (so that $dt = -\sin\theta \, d\theta$), we obtain

$$\tilde{\mu}_p = \int_{-1}^{1} T_p(t) \, \varphi(t) \, dt = \int_0^\pi \cos(p\theta) \, \varphi(\cos\theta) \, \sin\theta \, d\theta = \int_0^\pi \cos(p\theta) \, h(\theta) \, d\theta.$$

Since $\varphi \in L^1([-1,1])$, we have $h \in L^1(0,\pi)$ (indeed, $\sin\theta \le 1$ and $\varphi(\cos\theta)$ is integrable with respect to $d\theta$ after the change of variables). Therefore $\tilde{\mu}_p$ is the $p$-th cosine Fourier coefficient of an $L^1$ function, and by the Riemann–Lebesgue lemma it follows that $\tilde{\mu}_p \to 0$ as $p \to \infty$. Multiplying by $\|r_0\|^2$ gives $\mu_p \to 0$.

*(3)* From (2) we have $\tilde{\mu}_p = \int_0^\pi \cos(p\theta) \, h(\theta) \, d\theta$. Assume $h \in W^{q,1}(0,\pi)$. Integrating by parts once gives

$$\tilde{\mu}_p = \left[ \frac{\sin(p\theta)}{p} \, h(\theta) \right]_0^\pi - \frac{1}{p} \int_0^\pi \sin(p\theta) \, h'(\theta) \, d\theta.$$

The boundary term vanishes because $\sin(p\theta) = 0$ at $\theta = 0, \pi$. Hence,

$$|\tilde{\mu}_p| \le \frac{1}{p} \int_0^\pi |h'(\theta)| \, d\theta.$$

Repeating this argument $q$ times (alternating sin and cos) and using that the boundary terms always vanish (again due to $\sin(p\theta) = 0$ at 0 and $\pi$) yields

$$|\tilde{\mu}_p| \le \frac{1}{p^q} \int_0^\pi |h^{(q)}(\theta)| \, d\theta = \frac{C_q}{p^q}, \qquad C_q := \|h^{(q)}\|_{L^1(0,\pi)}.$$

Finally, $\mu_p = \|r_0\|^2 \tilde{\mu}_p$ implies $|\mu_p| \le \|r_0\|^2 C_q p^{-q}$. □

**Remark 4.** *Theorem 2 distinguishes between two fundamentally different regimes. In finite dimensions, where the spectral measure induced by $(A, r_0)$ is purely discrete, the Chebyshev moments $\mu_p$ are uniformly bounded but do not, in general, decay as $p \to \infty$; they may instead exhibit persistent oscillations. Decay properties arise only under additional regularity assumptions on the spectral measure, such as the presence of an absolutely continuous component with sufficient smoothness. Accordingly, any decay of the off-diagonal entries of the Gram matrix observed in practice should be interpreted as an average or empirical effect, rather than as a guaranteed asymptotic property in the finite-dimensional setting.*

*The contrast between the discrete and continuous settings has a precise quantitative form that makes the continuous framework not merely convenient but necessary. For a fixed $n \times n$ matrix with minimum angular eigenvalue separation $\delta_n = \min_{\ell \ne m} |\theta_\ell - \theta_m|$, a direct bound via Abel summation on the discrete cosine transform gives $|\mu_p| \le \pi W/(p\delta_n)$. For a sequence of PDE matrices under mesh refinement, $\delta_n = O(1/n)$, so this bound gives $|\mu_p| \le \pi W n/p$, which diverges as $n \to \infty$ for any fixed $p$ and is therefore useless at the scale for which the method is designed. The $W^{q,1}$ framework of Theorem 2 Part* (3) *gives $|\tilde{\mu}_p| \le C_q/p^q$ with $C_q$ depending on the spectral density but not on $n$. This bound*

*is uniform in $n$: it captures cancellation from eigenvalue distribution rather than from individual eigenvalue separation, and remains valid and sharp as $n \to \infty$. Every classical convergence bound for CG and Generalized Minimum Residual (GMRES) that invokes a condition number or a spectral interval implicitly operates in this continuous-density regime; the present analysis is consistent with that tradition.*

*In practice, however, the choice of preconditioner can influence the effective spectral distribution of the preconditioned operator. A robust preconditioner that clusters eigenvalues and reduces spectral outliers may promote cancellation effects in the Chebyshev moments, thereby yielding a Gram matrix that is empirically closer to diagonal and better conditioned. This improvement should be understood as a practical consequence of spectral regularization rather than as a theoretical guarantee of moment decay.*

**Corollary 3** (Structure of the normalized Chebyshev Gram matrix)**.** *Let $W$ be the Chebyshev Gram matrix, and let $W_c$ denote its diagonally normalized form. Then $W_c$ is SPD, has unit diagonal, and its off-diagonal entries satisfy*

$$|(W_c)_{ij}| \le \frac{1}{2}\big(|\tilde{\mu}_{|i-j|}| + |\tilde{\mu}_{i+j-2}|\big), \qquad i \neq j,$$

*where $\tilde{\mu}_p := \mu_p/\mu_0$ are the normalized Chebyshev moments. In particular, the off-diagonal entries are uniformly bounded by*

$$|(W_c)_{ij}| \le 1,$$

*and their magnitude typically decreases as $|i-j|$ increases when cancellation in the Chebyshev moments occurs.*

**Corollary 4** (Algebraic entry-wise decay under $W^{2,1}$ smoothness)**.** *Assume Theorem 2 (3) holds with $q = 2$, so $|\tilde{\mu}_p| \le C_2 p^{-2}$. Then the entries of the normalized Chebyshev Gram matrix $W_c$ satisfy*

$$|(W_c)_{ij}| \le \frac{C_2}{(|i-j|+1)^2}, \qquad i \neq j, \tag{12}$$

*where $C_2$ depends on the spectral density and initial residual, not on $s$ or $n$. The off-diagonal row sum satisfies*

$$\sum_{j \neq i} |(W_c)_{ij}| \le C_2 \sum_{d=1}^{\infty} \frac{1}{d^2} = \frac{\pi^2 C_2}{6}. \tag{13}$$

*Proof.* Apply Corollary 3 with $|\tilde{\mu}_p| \le C_2 p^{-2}$ for $p \ge 1$ from Theorem 2*(3)*. For $i \neq j$, both indices $|i-j| \ge 1$ and $i+j-2 \ge |i-j| \ge 1$, so

$$|(W_c)_{ij}| \le \tfrac{1}{2}\left(\frac{C_2}{|i-j|^2} + \frac{C_2}{(i+j-2)^2}\right) \le \frac{C_2}{|i-j|^2}.$$

Since $|i-j| \ge 1$ implies $|i-j|^2 \le (|i-j|+1)^2 \le 4\,|i-j|^2$, absorbing the factor of at most 4 into the constant $C_2$ (replacing $C_2$ by $4C_2$ and relabelling) gives

$$|(W_c)_{ij}| \le \frac{C_2}{(|i-j|+1)^2},$$

which is (12). Summing over $j \neq i$ and using $\sum_{d=1}^{\infty} d^{-2} = \pi^2/6$ gives (13), with $C_2$ understood as the (relabelled) constant. □

**Definition 1** (Clustered spectral density)**.** *The normalized spectral density $\varphi$ is said to be $(p_c, \delta, \Delta)$ clustered if there exist $p_c$ cluster centers $\nu_1 < \cdots < \nu_{p_c}$ in $[-1, 1]$ such that: (i) $\varphi$ is supported on $p_c$ intervals $I_a$ of half-width $\delta$ centered at $\nu_a$; (ii) the inter-cluster separation $\Delta := \min_{a \neq b} |\nu_a - \nu_b|$ satisfies $\Delta > 2\delta$; (iii) on each $I_a$, $\varphi|_{I_a} \in W^{2,1}(I_a)$ with $\|\varphi|''_{I_a}\|_{L^1} \leq M_a$. The cluster weights are $W_a = \int_{I_a} \varphi \, dt$ with $W_{\text{tot}} = \sum_a W_a = 1$.*

**Theorem 3** (Cluster separation and Gram decay)**.** *Let $\varphi$ be $(p_c, \delta, \Delta)$ clustered (Definition 1). Define $\mu_p^{\text{cl}} := \sum_{a=1}^{p_c} W_a T_p(\nu_a)$, the cluster-center moments. Then for all integers $p \geq 1$:*

$$|\tilde{\mu}_p - \mu_p^{\text{cl}}| \leq p\delta W_{\text{tot}}, \tag{14}$$

*and the cluster-center moments satisfy*

$$|\mu_p^{\text{cl}}| \leq \frac{C_\Delta}{p^2}, \qquad C_\Delta = \sum_{a=1}^{p_c} M_a + \frac{2W_{\text{tot}}}{\Delta^2}. \tag{15}$$

*Consequently, for $p \leq 1/(2\delta)$,*

$$|\tilde{\mu}_p| \leq \frac{C_\Delta}{p^2} + \tfrac{1}{2} W_{\text{tot}}, \tag{16}$$

*and the normalized Gram entries satisfy*

$$|(W_c)_{ij}| \leq \frac{C_\Delta}{(|i-j|)^2} + W_{\text{tot}} \tag{17}$$

*for all $|i-j| \leq 1/(2\delta)$, in particular for all step sizes $s \ll 1/\delta$. This bound is informative when $C_\Delta \ll 1$, which holds when $\Delta = O(1)$ and the intra-cluster smoothness constants $M_a$ are small. For $|i-j| \geq 2$ and $C_\Delta < 1$, the bound is strictly tighter than the uniform bound $|(W_c)_{ij}| \leq 1$ of Corollary 3.*

*Proof.* Write $\tilde{\mu}_p = \int_0^\pi \cos(p\theta) h(\theta) \, d\theta$. Decompose $h = h^{\text{cl}} + h^{\text{in}}$, where $h^{\text{cl}}$ places all cluster weight at center angles $\hat{\theta}_a = \arccos(\nu_a)$. For the intra-cluster residual: each spectral angle $\theta_\ell$ lies within $O(\delta)$ of some $\hat{\theta}_a$, and $|\cos(p\theta_\ell) - \cos(p\hat{\theta}_a)| \leq p|\theta_\ell - \hat{\theta}_a| \leq Cp\delta$. Summing over all eigenvalues gives (14).

For the cluster-center moments: the centers $\hat{\theta}_a$ have angular separation $\hat{\Delta} \geq 2\Delta/\pi$. Integrating by parts twice against the density on each cluster $I_a$, with $\|\varphi|''_{I_a}\|_{L^1} \leq M_a$ bounding the intra-cluster contribution and the inter-cluster separation $\Delta$ controlling cross terms, gives (15) with $C_\Delta$ as stated.

Combining (14) and (15): for $p \leq 1/(2\delta)$, $p\delta \leq 1/2$, giving (16). Corollary 3 then gives (17). □

**Remark 5** (Preconditioner quality as a Gram conditioning diagnostic)**.** *Theorem 3 makes Remark 4 precise by quantifying how the inter-cluster separation $\Delta$ of the preconditioned spectral density controls the constant $C_\Delta$ appearing in the entry-wise decay bound (17). The constant is*

$$C_\Delta = \sum_{a=1}^{p_c} M_a + \frac{2W_{\text{tot}}}{\Delta^2},$$

*where $M_a$ bounds the intra-cluster smoothness of $\varphi$ on the $a$-th cluster interval and $W_{\text{tot}} = 1$. The term $2/\Delta^2$ dominates when clusters are well separated, so $C_\Delta$ decreases as $\Delta$*

*increases. By Corollary 3, the off-diagonal entries of the normalized Chebyshev Gram matrix $W_c$ satisfy*

$$|(W_c)_{ij}| \le \frac{C_\Delta}{(|i-j|+1)^2}, \qquad i \neq j,$$

*so a smaller $C_\Delta$ implies faster off-diagonal decay and a Gram matrix closer to the identity. A Gram matrix close to the identity implies that the strictly lower triangular part $L$ satisfying $W = I+L+L^\top$ is small in norm, and by the contraction argument of Section 3.1 a small number of FGS sweeps suffices to satisfy the inexact Krylov tolerance (1). A good algebraic multigrid preconditioner clusters the eigenvalues of $M^{-1}A$ around $p_c = O(1)$ centers with $\Delta = O(1)$, so $C_\Delta = O(1)$ uniformly in $n$. The entry-wise decay bound then holds with an $O(1)$ constant independently of the dimension of the linear system, and a fixed step size $s = O(1)$ together with a fixed number of FGS sweeps are justified across all problem sizes accessible to the preconditioner. A preconditioner with larger $\Delta$ permits a smaller $s$ while maintaining the same Gram solve accuracy, which directly reduces the number of global reductions per outer iteration and therefore lowers communication cost.*

## 3.2 Connection between FGS and MGS

The behavior of the FGS iteration can be understood through a classical equivalence with the Modified Gram–Schmidt (MGS) orthogonalization process. This connection clarifies the stability properties of FGS when applied to Gram systems.

**Theorem 4** (Ruhe's equivalence [22])**.** *Let $P = [p_1, \dots, p_s] \in \mathbb{R}^{n\times s}$ have linearly independent, column-normalized vectors, and let $W = P^\top P$ be its Gram matrix, so that*

$$W = I + L + L^\top,$$

*with $L$ strictly lower triangular.*

*Consider one forward Gauss–Seidel sweep applied to the Gram system*

$$W\alpha = e_1, \qquad \alpha^{(0)} = 0,$$

*where $e_1 \in \mathbb{R}^s$ is the first canonical basis vector. This right-hand side isolates the orthogonalization of the first column $p_1$ against the remaining columns of $P$.*

*Let $\alpha^{(1)}$ denote the vector obtained after one sweep. Then the linear combination*

$$\tilde{p}_1 := P\alpha^{(1)}$$

*satisfies*

$$\tilde{p}_1 = p_1 - \sum_{j=2}^{s} \langle p_j, p_1\rangle\, p_j,$$

*which is exactly one pass of the Modified Gram–Schmidt (MGS) orthogonalization of $p_1$ with respect to $p_2, \dots, p_s$.*

*Proof.* Since $W_{ij} = \langle p_i, p_j\rangle$, we have $L_{ji} = \langle p_j, p_i\rangle$ for $j > i$. A forward Gauss–Seidel sweep solves

$$(I + L)\alpha^{(1)} = e_1.$$

By forward substitution,

$$\alpha_1^{(1)} = 1, \qquad \alpha_j^{(1)} = -\sum_{i=1}^{j-1} \langle p_j, p_i\rangle\, \alpha_i^{(1)}.$$

Since $\alpha_1^{(1)} = 1$, it follows that

$$\alpha_j^{(1)} = -\langle p_j, p_1 \rangle, \quad j = 2, \ldots, s,$$

and therefore

$$P\alpha^{(1)} = p_1 - \sum_{j=2}^{s} \langle p_j, p_1 \rangle \, p_j,$$

which is exactly one MGS pass. □

**Extension to the $A$-inner product.** The equivalence extends directly to non-Euclidean inner products. Let the columns of $Q \in \mathbb{R}^{n \times s}$ be $A$-normalized, so that $q_j^\top A q_j = 1$. Then the Gram matrix

$$W = Q^\top A Q$$

represents the matrix of $A$-inner products among the search directions.

One forward Gauss–Seidel sweep applied to

$$W\alpha = e_1$$

produces a vector $Q\alpha^{(1)}$ that coincides with one pass of Modified Gram–Schmidt in the $A$-inner product. Thus, for the right-hand side $e_1$, one FGS sweep performs an implicit $A$-orthogonalization step.

**Implications for stability.** This structural equivalence has important stability consequences. Theorem 4 establishes the FGS-MGS equivalence for the right-hand side $e_1$. For the general right-hand sides $m = Q^\top r$ and $m = -Q^\top A Z_{\text{new}}$ arising in PCG-S, FGS produces a different linear combination of the basis vectors; nevertheless, the FGS iteration matrix $G = -(I + L)^{-1} L^\top$ is the same in all cases, and the stability of the iteration is governed by the same spectral norm $\|L^\top (I + L)^{-1}\|_2$ as in the MGS analysis. The loss of $A$-orthogonality therefore behaves analogously to MGS.

In particular, classical finite-precision analyses of MGS in non-standard inner products [26, 27, 23, 21, 17] document that the loss of orthogonality is governed by $\kappa(A^{1/2}Q)$, which is $O(s)$ for Chebyshev bases under the regularity hypothesis of Corollary 5, provided the Gram matrix remains moderately conditioned.

Consequently, when FGS is applied to the Gram systems arising in PCG-S, it inherits the same stability properties as $A$-MGS. The inner iteration is therefore not merely a stationary solver, but an implicit orthogonalization process whose numerical behavior is governed by well-understood MGS bounds.

**Lemma 2** (Gram condition number and $A^{1/2}Q$ condition number)**.** *Let $Q \in \mathbb{R}^{n \times s}$ have full column rank, let $A \in \mathbb{R}^{n \times n}$ be SPD, and let $W = Q^T A Q$ be the $A$-Gram matrix. Normalize $Q$ so that* $\operatorname{diag}(W) = I$ *(each column of $Q$ has unit $A$-norm). Then*

$$\kappa_2(A^{1/2}Q)^2 = \kappa_2(W),$$

*and consequently $\kappa_2(A^{1/2}Q) = \kappa_2(W)^{1/2}$, where $\kappa_2(\cdot)$ denotes the condition number in the spectral norm.*

*Proof.* Write $F = A^{1/2}Q$. Then $W = F^T F$. The singular values of $F$ are the square roots of the eigenvalues of $W$, so $\kappa_2(F)^2 = \lambda_{\max}(W)/\lambda_{\min}(W) = \kappa_2(W)$. □

**Corollary 5** (Stability inheritance in the $A$-inner product)**.** *Let $Q \in \mathbb{R}^{n\times s}$ be the block Krylov basis of Algorithm 1, normalized so that each column has unit $A$-norm. By Lemma 2, $\kappa_2(A^{1/2}Q) = \kappa_2(W)^{1/2}$. Theorem 2 establishes moment decay of the Chebyshev Gram entries when the spectral measure $d\mu(\lambda)$ of $A$ is absolutely continuous with a Hölder-regular density on $[\lambda_{\min}, \lambda_{\max}]$. Under this regularity hypothesis, the condition number $\kappa_2(W) = O(s^2)$ for moderate $s$ (following Philippe and Reichel [20], whose quadratic growth bound applies to the Chebyshev-based Gram matrix under spectral regularity), and therefore*

$$\kappa_2(A^{1/2}Q) = O(s).$$

*The loss of $A$-orthogonality then satisfies $\|I - Q^\top AQ\|_2 = O(su)$ by the standard finite-precision MGS analysis [21, 17], where $u$ denotes the unit roundoff.*

## 3.3 Numerical Experiments

In this section we assess experimentally the effect of the inexact FGS solution of the reduced Gram systems within the PCG-S framework. We consider as benchmark, the linear systems arising from a 27-point finite difference discretization of the 3D Poisson equation on a cube with Dirichlet boundary conditions. The problem was solved on 64 GPUs and has a total size of $64 \times 200^3 = 5.12 \times 10^8$. The objective is to verify that a small, fixed number of inner sweeps is sufficient to preserve the convergence behavior predicted by the analysis of Section 3. In particular, we examine the empirical structure of the Chebyshev Gram matrices arising during the iteration, the decay of the Gram-solve residual (Figure 2), and the resulting outer PCG-S convergence histories (Figure 3).

Figure 1 shows representative Gram matrices $W_k = Q_k^T AQ_k$ with step size $s = 10$ at successive outer iterations.

This empirical behavior is consistent with the moment representation derived in Section 3. As the iteration evolves, higher-order Chebyshev moments tend to exhibit stronger cancellation, leading to a more diagonally concentrated Gram matrix.

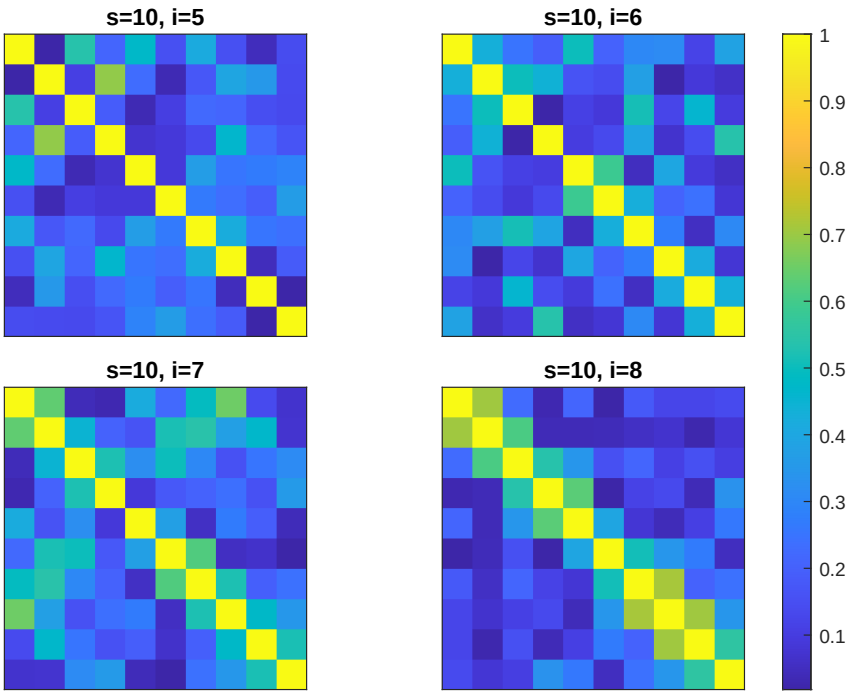


Figure 1: Empirical structure of the Chebyshev Gram matrices for the test problem considered in this section with step size $s = 10$. The panels correspond to outer iterations $k = 5, \ldots, 8$ of the PCG-S method. A progressive concentration of the matrix entries around the diagonal can be observed as the iteration proceeds.

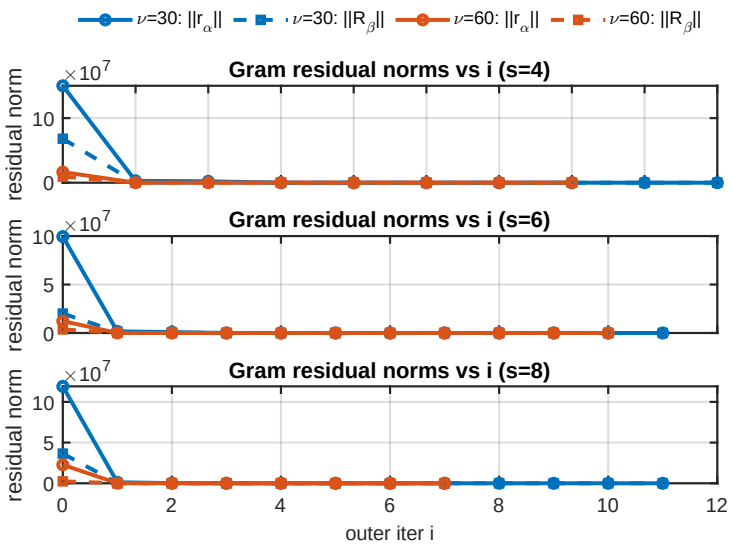


Figure 2: Gram-solve relative residuals $\|r_\alpha\|_2/\|m\|_2$ (for the $\alpha$ system) and $\|R_\beta\|_F/\|M\|_F$ (for the $\beta$ system) versus outer iteration, for two values of the FGS sweep count $\nu$ and several step sizes $s$, on the 27-point Poisson problem with $5.12 \times 10^8$ DOFs on 64 GPUs.

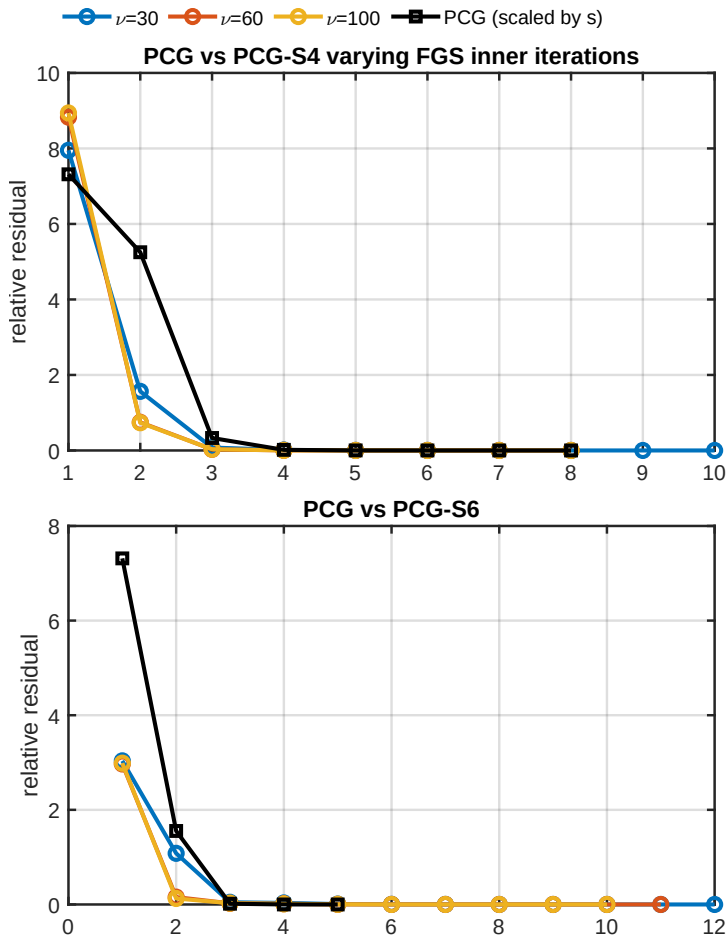


Figure 3: PCG-S outer relative residual $\|r^{(k)}\|/\|b\|$ versus outer iteration, for two values of the FGS sweep count $\nu$ and step sizes $s \in \{4, 6\}$, compared to classical PCG and the Cholesky-based Gram solve. Problem: 27-point Poisson, $5.12 \times 10^8$ DOFs on 64 GPUs.

Figure 2 reports the directly computed residual norms of the Gram solves for different numbers of FGS inner iterations $\nu$ and step sizes $s$. We explicitly evaluate

$$\|r_\alpha\|_2 = \|\mathrm{rhs}_\alpha - W_k\alpha_k\|_2, \qquad \|R_\beta\|_{fro} = \|\mathrm{rhs}_\beta - W_k\beta_k\|_{fro},$$

at each outer iteration.

The residuals exhibit an immediate decay toward zero, typically reaching the order of $10^{-2}$ already after the second outer iteration. At the same time, increasing the step size $s$ reduces the total number of outer iterations, which remains on the order of a few tens. These results confirm that the inexact Gram solves satisfy the inexact Krylov condition (1), ensuring that the outer convergence mechanism is preserved while using a fixed and moderate number of FGS sweeps.

Figure 3 reports the outer PCG-S relative residual histories. For $\nu \geq 30$, the convergence curves are essentially indistinguishable and closely match both classical PCG and the Cholesky-based Gram solve. This confirms that a small, fixed number of FGS sweeps preserves the outer convergence behavior, in agreement with the inexact Krylov requirement in condition (2).

No instability is observed as $s$ increases, which is consistent with the quadratic conditioning growth $\kappa_2(W) = \mathcal{O}(s^2)$ for Chebyshev Gram matrices and with the stability inheritance result of Corollary 5. Overall, the experiments validate the theoretical analysis of Section 3.

# 4 Practical Implementation

The PCG-S method described in Algorithms 1 and 2 has been implemented in the `BootCMatchGX` framework, a distributed NVIDIA multi-GPU software environment for large-scale sparse linear algebra. The implementation combines MPI-based domain decomposition across nodes with CUDA-based acceleration on each GPU.

The solver layer is modular and decoupled from the matrix storage format, the preconditioner implementation and the communication backend. This abstraction enables the PCG-S algorithm to operate independently of the underlying preconditioner and facilitates future extensions without modifying the Krylov engine.

The Matrix Power Kernel (Algorithm 2), responsible for generating the Chebyshev block basis, relies on a distributed SpMV implementing explicit communication–computation overlap. Given the row-wise domain decomposition, halo exchanges are required at each SpMV application. In our implementation, non-blocking MPI communications are initiated prior to launching the local GPU kernel. While boundary data are being transferred, the interior rows are processed on the device. After communication completion, boundary contributions are finalized. This strategy follows the standard overlap paradigm for distributed SpMV and is particularly effective in strong-scaling regimes where communication latency dominates arithmetic cost. Within each MPK cycle, SpMV and preconditioner applications alternate.

The current implementation provides an Algebraic MultiGrid (AMG) preconditioner based on aggregation of unknowns, driven by the so-called *Compatible Weighted Matching* (see [11, 1] for details), already available in `BootCMatchGX`. However, the solver architecture exposes a generic preconditioner interface. Any future preconditioner that conforms to this interface can be seamlessly integrated into the PCG-S framework without modifying Algorithms 1 or 2. Thus, the s-step formulation remains agnostic to the specific choice of preconditioner, and the communication-reduction strategy is orthogonal to preconditioning design.

All block linear algebra operations arising in PCG-S are formulated in terms of small dense matrix kernels to maximize arithmetic intensity on GPUs. In particular, local operations are performed using the GEMM and GEMV routines from the cuBLAS library. These kernels are used for the block operations in Algorithm 1, including updates of the approximate solution and residual (lines 7–8), construction of the local Gram contributions and right-hand sides (lines 5 and 13), and block recurrences (line 15). Recasting vector recurrences as dense block operations enables efficient utilization of current tensor cores and high-throughput GPU pipelines, significantly increasing computational efficiency relative to classical scalar CG updates. All such operations are executed locally on the device, avoiding unnecessary host-device transfers and increasing effective flop utilization.

The reduced Gram matrix $W \in \mathbb{R}^{s\times s}$ is assembled from products between local vector blocks. Each process computes its local contribution via cuBLAS GEMM, and an MPI all-reduce combines these contributions to obtain the global matrix $W$, replicated on all ranks. The FGS iteration used to approximate the solutions of the related systems (lines 6 and 14) is executed redundantly on each CPU. This design is justified by the small dimension of the Gram system ($s \leq 10$ in practical regimes), the negligible cost of $\nu(s^2 + 2s)$ flops relative to the CPU-side global reduction cost, and the fact that the CPU is already engaged during global reductions.

After completion of the FGS iteration, the coefficient vectors and matrices are trans-

ferred back to the GPU and used for block updates. Overall, the implementation is explicitly designed to operate in the regime where latency dominates arithmetic cost, thereby exploiting the asymptotic advantages predicted by the strong and weak scaling analyses of the next section.

## 4.1 Performance Model

In large-scale GPU-accelerated environments, the performance of Krylov subspace methods is increasingly dominated by communication costs rather than arithmetic throughput. A quantitative performance model is therefore essential to characterize the trade-off between reduced global synchronization and increased local computation introduced by the s-step formulation. In this section, we derive a latency–bandwidth based model that captures these effects and predicts the scalability regime in which the proposed method becomes advantageous over classical PCG.

Let $W_{\text{SpMV}}$ and $W_{\text{prec}}$ denote the cost of one parallel sparse matrix–vector multiplication and one preconditioner application, respectively. Let $W_{\text{axpy}}$, $W_{\text{dot}}$, and $W_{\text{allreduce}}$ be the costs of one vector update (axpy), one dot product, and one global reduction (required by parallel dot products), respectively.

Then, the cost of a single iteration of the PCG method can be approximated as

$$W_{\text{PCGiter}} \approx W_{\text{SpMV}} + W_{\text{prec}} + 3W_{\text{axpy}} + 2W_{\text{dot}} + 2W_{\text{allreduce}}.$$

For the PCG-S method with a Chebyshev-based MPK kernel and $\nu$ FGS sweeps on the Gram system, the cost of one outer iteration is

$$\begin{aligned} W_{\text{PCGSiter}}(\nu) \approx\ & s \cdot (W_{\text{SpMV}} + 2W_{\text{axpy}}) + s \cdot W_{\text{prec}} \\ & + \left(\frac{s(s+1)}{2} + s\right) W_{\text{dot}} + s^2 W_{\text{dot}} + 2W_{\text{allreduce}} + \nu W_{\text{FGSsweep}} + 2W_{\text{matupdates}}, \end{aligned}$$

where $W_{\text{matupdates}}$ accounts for local rectangular matrix updates (line 15 in Algorithm 1).

By grouping equivalent terms, we obtain

$$\begin{aligned} W_{\text{PCGSiter}}(\nu) \approx\ & sW_{\text{SpMV}} + sW_{\text{prec}} + 2sW_{\text{axpy}} + \tfrac{3}{2}(s^2+s)W_{\text{dot}} \\ & + 2W_{\text{allreduce}} + \nu W_{\text{FGSsweep}} + 2W_{\text{matupdates}}. \end{aligned}$$

If we explicitly account for the floating–point operations of local vector and matrix updates, which are parallel and do not require inter-process communication, the costs for $s$ iterations of PCG and the corresponding cost of 1 (outer) iteration of PCG-S, for a global problem of dimension $n$, can be rewritten as

$$\begin{aligned} s \cdot W_{\text{PCGiter}} &\approx s \cdot W_{\text{SpMV}} + s \cdot W_{\text{prec}} + 2s \cdot W_{\text{allreduce}} + 6sn \cdot \text{flop} + 2sn \cdot \text{flop}, \\ W_{\text{PCGSiter}}(\nu) &\approx sW_{\text{SpMV}} + sW_{\text{prec}} + 4sn \cdot \text{flop} + \tfrac{3}{2}(s^2+s)n \cdot \text{flop} + 2W_{\text{allreduce}} \\ &\quad + \nu(s^2+2s) \cdot \text{flop} + 2(s^2+s)n \cdot \text{flop}. \end{aligned}$$

Grouping the purely local (non–communicating) operations yields

$$\begin{aligned} W_{\text{PCGSiter}}(\nu) \approx\ & sW_{\text{SpMV}} + sW_{\text{prec}} + 2W_{\text{allreduce}} \\ & + \tfrac{7}{2}(s^2+s)n \cdot \text{flop} + \nu(s^2+2s) \cdot \text{flop}. \end{aligned}$$

Note that in our parallel implementation, FGS sweeps are replicated across all parallel tasks. Therefore, their cost $\nu(s^2 + 2s)$ flop represents a *sequential overhead*. In contrast, the cost of parallel operations, i.e., vector and matrix updates which are executed concurrently by all tasks, increases quadratically with $s$.

Let $t_{\text{flop}}$ denote the execution time of one double–precision flop on a single processor, and let us adopt the standard $(\alpha_{\text{lat}}, \beta)$ latency–bandwidth model to estimate communication time. Assuming that the time for one MPI allreduce among $P$ processors can be approximated as

$$T_{\text{allreduce}} \approx \alpha_{\text{lat}} \log_2 P,$$

the iteration times on P processes can be expressed as

$$T_{s,\text{PCGiter}} \approx sT_{\text{SpMV}} + sT_{\text{prec}} + 2s\,\alpha_{\text{lat}} \log_2 P + \frac{8sn}{P}\, t_{\text{flop}},$$

$$T_{\text{PCGSiter}}(\nu) \approx sT_{\text{SpMV}} + sT_{\text{prec}} + 2\,\alpha_{\text{lat}} \log_2 P + \frac{\frac{7}{2}(s^2+s)n}{P}\, t_{\text{flop}} + \nu(s^2+2s)\, t_{\text{flop}},$$

where $T_{\text{SpMV}}$ and $T_{\text{prec}}$ are the execution times for one parallel SpMV and for one parallel application of a preconditioner, respectively.

**Interpretation of the difference.**

$$\begin{aligned}\Delta(P, s, \nu) &= T_{\text{PCGSiter}}(\nu) - T_{s,\text{PCGiter}} \\ &= 2\alpha_{\text{lat}}\,(1-s)\log_2 P + \frac{s(7s-9)}{2}\,\frac{n}{P}\, t_{\text{flop}} + \nu(s^2+2s)\, t_{\text{flop}} \qquad (18)\end{aligned}$$

represents the difference between the time required for one outer iteration of the PCG-S algorithm and $s$ consecutive classical PCG iterations. A negative value of $\Delta$ indicates that one iteration of PCG-S is faster than $s$ iterations of the classical PCG.

**Communication term.** The first component,

$$2\alpha_{\text{lat}}\,(1-s)\log_2 P,$$

quantifies the variation in global communication cost. In the classic PCG method, each iteration involves two global reductions, whereas PCG-S performs only two reductions per outer iteration, corresponding to $s$ PCG iterations. For $s > 1$, this term becomes *negative*, indicating that PCG-S reduces the number of global synchronizations by a factor of $s$. Consequently, this component favors PCG-S in large-scale parallel systems where latency dominates the overall execution time.

**Computational term.** The second component,

$$\frac{s(7s-9)}{2}\,\frac{n}{P}\, t_{\text{flop}},$$

represents the difference in distributed floating-point workload. It is *positive* for $s > 2$, indicating that one iteration of PCG-S requires more local arithmetic operations than $s$ iterations of PCG. This additional cost arises from the extra dot products needed to form the Gram systems and recurrence relations within the $s$-step Krylov basis. Consequently, this term tends to increase $\Delta$, penalizing PCG-S for increasing $s$.

**Gram solve overhead.** The last component,

$$\nu(s^2 + 2s)\, t_{\text{flop}},$$

captures the overhead for applying $\nu$ FGS iterations to the Gram system. It is always *positive*, scales quadratically with $s$, and grows linearly with $\nu$, therefore contributing an additional sequential overhead to the total runtime of $s$-step PCG.

In summary, $\Delta(P, s, \nu)$ highlights the trade-off between *reduced communication latency* (first term, beneficial) and *increased local computation* (second and third terms, detrimental). As expected, PCG-S can become advantageous when communication latency dominates over local computation, i.e., for large $P$ and high-latency parallel architectures.

**Parametric interpretation under strong scaling.** In the strong–scaling regime, the global problem size $n$ is fixed while the number of processes $P$ increases, so that each process handles a smaller local workload $c(P) = n/P$. Figure 4 shows the behavior of $\Delta_{\text{strong}}(P, s, \nu)$ for $\nu = 30$, $n = 500^3$.

As $P$ increases from 32 to 512, the computational contribution in $\Delta_{\text{strong}}$,

$$\frac{s(7s-9)}{2}\,\frac{n}{P}\,t_{\text{flop}} + \nu(s^2 + 2s)\, t_{\text{flop}},$$

decreases approximately as $1/P$, reflecting the reduced local arithmetic workload per process. Conversely, the communication term,

$$2\alpha_{\text{lat}} \log_2 P\,(1 - s),$$

grows logarithmically with $P$, since the cost of global reductions increases with the depth of the communication tree. Because this term is *negative* for $s > 1$, it represents a latency *reduction* that becomes increasingly dominant at large process counts.

The combined effect produces a monotonic decrease in $\Delta_{\text{strong}}$ as $P$ grows, eventually leading to a crossover point where $\Delta_{\text{strong}} < 0$, and the PCG-S algorithm becomes more efficient than the classical PCG. This transition occurs at larger process counts for larger $s$, as the enhanced communication savings of PCG-S increasingly compensate for its greater local computational cost.

Overall, the strong–scaling results confirm that for small $P$ or small steps $s$, the classical PCG remains competitive; however, at large $P$ and high $\alpha_{\text{lat}}/t_{\text{flop}}$ ratios, the reduced synchronization cost suggests that PCG-S becomes increasingly advantageous.

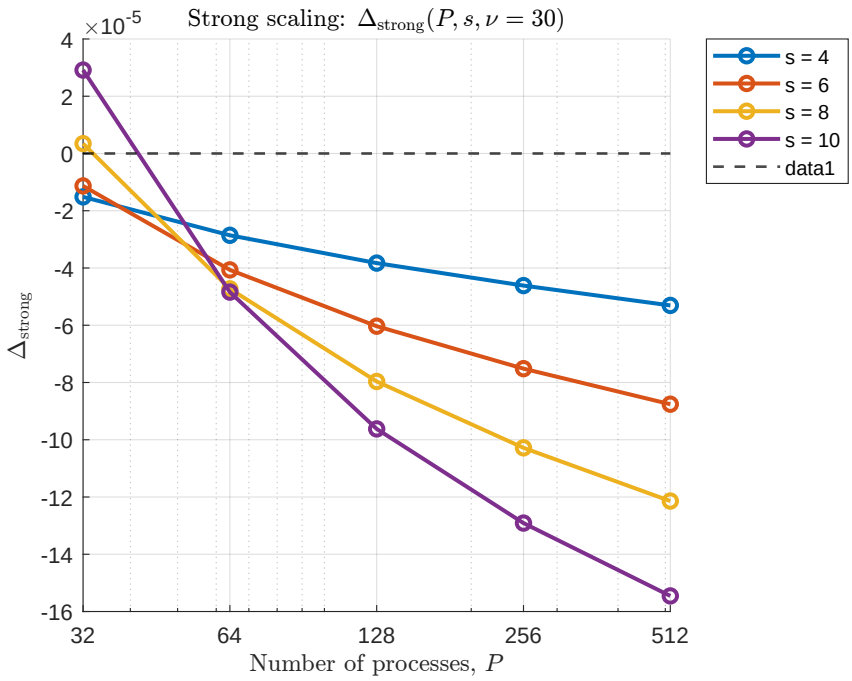


Figure 4: Strong–scaling behavior of $\Delta_{\text{strong}}(P, s, \nu = 30)$ as a function of the number of processes $P$ for several step sizes $s$, with fixed $n = 500^3$. The dashed line marks $\Delta_{\text{strong}} = 0$.

**Parametric interpretation under weak scaling.** Under weak scaling, where $n = cP$ and each processor handles a fixed local problem size $c$, the difference in (18) becomes

$$\Delta_{\text{weak}}(P, s, \nu) = 2\alpha_{\text{lat}}\,(1 - s)\log_2 P + \frac{c\,s(7s - 9)}{2}\,t_{\text{flop}} + \nu(s^2 + 2s)\,t_{\text{flop}}.$$

The sign of $\Delta_{\text{weak}}$ is determined by the competition between:

1. the *communication gain* of the PCG-S method, given by $2\alpha_{\text{lat}}\,(1 - s)\log_2 P < 0$ for $s > 1$, which represents the latency reduction from fewer global synchronizations; and

2. the *computational penalty* of PCG-S, $\frac{c\,s(7s-9)}{2}\,t_{\text{flop}} + \nu(s^2 + 2s)\,t_{\text{flop}}$, arising from the additional local arithmetic operations and sequential overhead.

PCG-S becomes asymptotically advantageous ($\Delta_{\text{weak}} < 0$) if and only if the communication savings dominate the extra computation, that is,

$$2\alpha_{\text{lat}}\,(s - 1)\log_2 P \;>\; \frac{c\,s(7s - 9)}{2}\,t_{\text{flop}} + \nu(s^2 + 2s)\,t_{\text{flop}}.$$

Solving for $P$ yields the critical process count beyond which PCG-S outperforms the classical PCG:

$$\log_2 P(s, \nu) = \frac{t_{\text{flop}}\left[\frac{c\,s(7s-9)}{2} + \nu(s^2 + 2s)\right]}{2\alpha_{\text{lat}}\,(s - 1)}, \qquad s > 1. \tag{19}$$

The values in Table 1 represent the minimum number of processes $P_{\text{crit}}(s, 30)$ required for the PCG-S method to become faster than the classical PCG in the weak-scaling

| $s$ | $\log_2 P_{\text{crit}}(s, 30)$ | $P_{\text{crit}}(s, 30)$ |
|---|---|---|
| 2 | 2 | 4 |
| 3 | 3.6 | 12 |
| 4 | 5.067 | 34 |
| 5 | 6.5 | 91 |
| 6 | 7.92 | 242 |
| 7 | 9.333 | 645 |
| 8 | 10.743 | 1714 |
| 9 | 12.15 | 4545 |
| 10 | 13.556 | 12040 |

Table 1: Critical process count $P_{\text{crit}}(s, 30)$ under weak scaling ($c = 200^3$, $\alpha_{\text{lat}} = 10^{-6}$ s, $t_{\text{flop}} = 10^{-13}$ s). Values below correspond to the crossover where $\Delta = 0$; for $P > P_{\text{crit}}$, one iteration of PCG-S becomes faster than $s$ iterations of PCG.

regime, under the model's assumptions on $\alpha_{\text{lat}}$ and $t_{\text{flop}}$. For $P > P_{\text{crit}}$, the reduction in global communication outweighs the additional local floating-point work, leading to $\Delta < 0$ (PCG-S faster). As noted in Section 6.1, the model underestimates communication costs relative to measured data; the actual crossover process counts are therefore likely lower than (more favorable than) those in the table.

As $s$ increases, $P_{\text{crit}}$ grows rapidly, approximately quadratically with $s$. This behavior reflects the trade-off between communication savings, which scale linearly with $s$, and computational overhead, which scales as $s^2$ due to the extra local operations in PCG-S. For small step sizes ($s = 2$–$5$), the crossover occurs at relatively modest parallel scales (tens of processes). For larger $s$, however, the crossover shifts to high process counts ($10^3$–$10^4$ processes), meaning that the communication advantage only becomes dominant on massively parallel systems.

In summary, the results confirm that the PCG-S method is advantageous in high-latency, large-scale environments, while for small $s$ or low process counts, the classical PCG remains competitive.

As also shown in Figure 5 the increasing dominance of the communication term at large process counts illustrates that a large latency-to-compute ratio, $\alpha_{\text{lat}}/t_{\text{flop}}$, favors the PCG-S method for sufficiently large $P$.

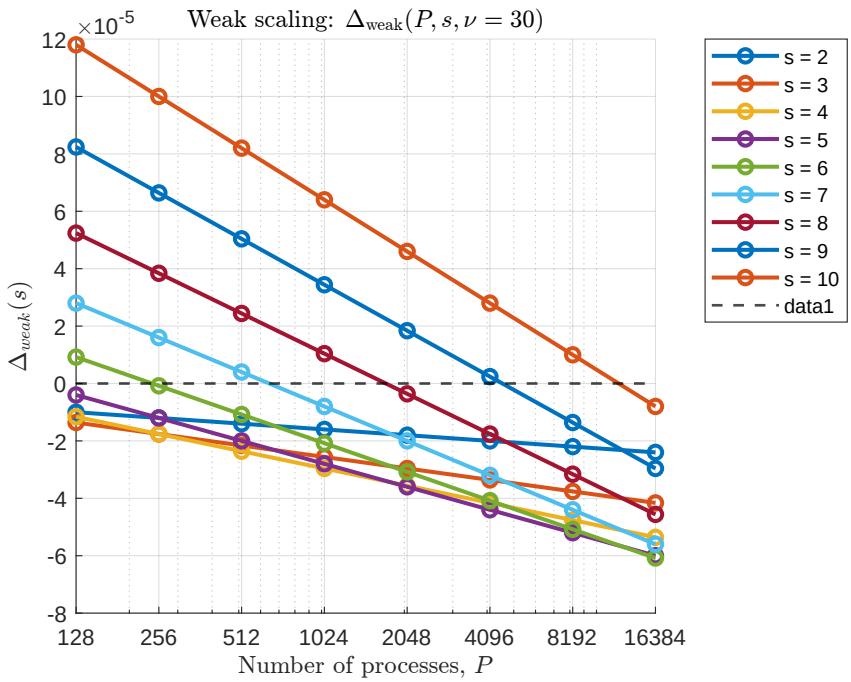


Figure 5: Weak–scaling behavior of $\Delta_{\text{weak}}(P, s, \nu = 30)$ versus the number of processes $P$, for several step sizes $s$, with scaling factor $c = 200^3$. The dashed line marks $\Delta_{\text{weak}} = 0$.

# 5 Related Work

Reducing global synchronization costs is a central challenge for Krylov subspace methods on modern large-scale architectures.

One class of approaches reduces the frequency of global synchronization. The $s$-step CG method, originally introduced by Chronopoulos and Gear [8, 7], groups several consecutive Krylov iterations into a single outer iteration, reducing the number of global reductions by a factor of $s$. This idea was later formalized within the broader framework of communication-avoiding (CA) Krylov methods by Hoemmen and Demmel [16, 12], where classical Krylov recurrences are reorganized so as to minimize synchronization while preserving the underlying Krylov sequence in exact arithmetic. A related but conceptually distinct strategy is followed by enlarged Krylov subspace methods [14, 15], which generate multiple search directions per iteration by expanding the approximation space, often through domain decomposition or multiple starting vectors.

A well-known limitation of early $s$-step and CA-CG formulations is their sensitivity to finite-precision effects. When monomial bases are used, the conditioning of the associated Gram matrices grows rapidly with $s$, which restricts practical step sizes. Moreover, the Chronopoulos–Gear variant reduces the number of global reductions by introducing auxiliary recurrence relations for dot products and Gram quantities; while effective in reducing synchronization, these additional recurrences increase algebraic coupling among quantities and may amplify rounding errors. Several works therefore investigated strategies to improve the numerical robustness of reduced-synchronization Krylov methods. Hoemmen [16] discussed the use of better-conditioned polynomial bases, such as Chebyshev or Newton polynomials, while Carson and collaborators studied adaptive $s$-step strategies and deflation or augmentation techniques for CA-CG [3, 5]. Mixed-precision variants of $s$-step Lanczos and CG have also been analyzed [4], where higher precision is used in the Gram matrix formation to mitigate conditioning issues. Although effective numerically,

approaches relying on quadruple precision are difficult to reconcile with the performance characteristics of modern accelerator-based architectures, where such arithmetic is typically emulated in software and introduces substantial computational overhead.

A complementary line of research aims instead to hide communication latency through pipelining. Pipelined CG methods reorganize the classical recurrences so that global reductions can be overlapped with sparse matrix–vector products and preconditioner applications [13]. While these methods significantly improve strong scaling, their multi-term recurrences may amplify rounding errors and reduce the maximal attainable accuracy in finite precision [6]. Stabilized pipelined variants have therefore been proposed to mitigate error propagation while preserving communication-hiding properties [9, 10].

Beyond algorithmic formulations, several works have investigated scalable implementations of these ideas on distributed-memory systems. Pipelined CG variants for large-scale architectures overlap global reductions with sparse matrix–vector products and preconditioner applications, thereby reducing idle time caused by synchronization [29]. Other implementations combine pipelining with $s$-step formulations to simultaneously reduce and hide communication costs, overlapping the construction of block Krylov bases with the evaluation of global reductions [28]. More general frameworks integrating pipelining with communication-avoiding $s$-step methods have also been proposed to improve scalability on large parallel systems [18, 19]. To the best of our knowledge, however, no previous work has provided an available fully distributed multi-GPU implementation of preconditioned $s$-step CG together with a large-scale experimental assessment. In this respect, the present work complements the existing literature by combining a numerically stabilized Chebyshev-based formulation, an inexact FGS Gram solve, and an implementation explicitly designed for modern multi-GPU architectures.

We adopt an $s$-step formulation that remains close to the classical PCG algorithm while avoiding auxiliary recurrence-based updates of the Gram matrix and long multi-term recurrences typical of pipelined approaches. The reduced systems are formed explicitly at each outer iteration, limiting error propagation while preserving the algebraic structure of classical PCG. Our approach exploits the structural properties of Chebyshev-based Gram matrices to improve conditioning and enables stable inexact solves of the reduced systems through FGS iterations in standard double precision. The theory of inexact Krylov methods [30] provides conditions under which such approximate inner solves do not compromise the convergence of the outer iteration. Our approach is inspired by recent work on low-synchronization projected solves in GMRES [24], where iterated Gauss–Seidel iterations were shown to provide an effective alternative to dense factorizations in communication-avoiding formulations.

# 6 Performance Results at Large Scale

We report results for our multi-GPU implementation of preconditioned $s$-step CG available in `BootCMatchGX`. Experiments were conducted on the Leonardo supercomputer (ranked 10th in the November 2025 Top500 list; BullSequana XH2000, Xeon Platinum 8358 32C 2.6 GHz, NVIDIA A100 SXM4 64 GB, quad-rail NVIDIA HDR100 InfiniBand) and on MareNostrum 5 at the Barcelona Supercomputing Center (accelerated partition ranked 14th in the November 2025 Top500 list; BullSequana XH3000, Intel Xeon Platinum 8460Y+ 32C 2.3 GHz, NVIDIA H100 SXM 64 GB, InfiniBand NDR), depending on resource availability.

The choice of linear system sizes and step sizes $s$ is guided by the theoretical model of Section 4.1 and by the maximum scale currently accessible on these systems. Further validation of the asymptotic predictions, including larger step sizes, will require benchmark-scale allocations planned for future work.

Strong and weak scalability are evaluated using linear systems arising from the standard 3D Poisson benchmark: matrix $A$ corresponds to the 27-point finite-difference discretization of the Poisson equation on the unit cube (as in HPCG), with Dirichlet boundary conditions and unit right-hand side. Matrices are row-partitioned across GPUs, mapping the 3D domain onto a 3D MPI process grid with one GPU per task.

## 6.1 Strong Scalability

In this section we report strong-scaling results obtained on MareNostrum 5. The Gram systems are solved using $\nu = 30$ iterations of the FGS method. Experiments are performed on a problem of size $500^3$ DOFs, using between 32 and 512 GPUs.

Our primary goal is to compare the CG-S method with the classical CG algorithm. To isolate the impact of global communication per iteration and assess the effect of the $s$-step formulation, we consider the unpreconditioned case and fix the number of (outer) iterations to $k_{\max} = 20$. In the unpreconditioned setting, the preconditioner is formally set to the identity matrix, $M = I$, so that $M^{-1}$ reduces to the identity operator and no preconditioning is applied within the MPK algorithm.

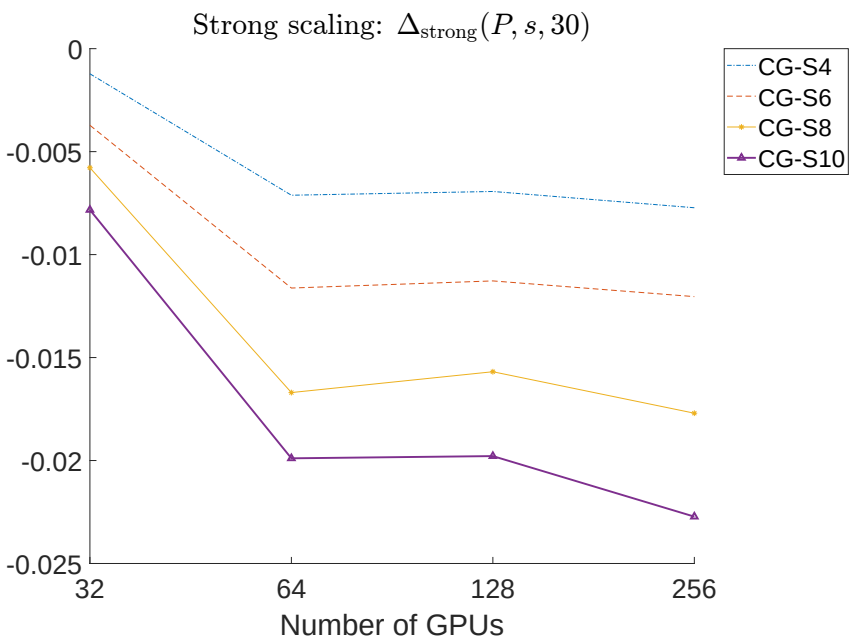


Figure 6: Strong–scaling behavior of $\Delta_{\text{strong}}(P, s, \nu = 30)$ with fixed $n = 500^3$

Figure 6 reports the strong-scaling indicator $\Delta_{\text{strong}}$ measured on MareNostrum 5 for the CG-S variants, with different values of $s$, as a function of the number of GPUs. For $P = 32$, the cost model predicts positive values of $\Delta_{\text{strong}}$ for $s \geq 6$, suggesting that the additional computational work of the $s$-step formulation should dominate at this scale. In contrast, the measured data show that $\Delta_{\text{strong}}$ is already negative in this regime. Moreover, its magnitude is approximately two orders of magnitude smaller than predicted, indicating that communication costs are significantly underestimated by the model. This suggests that communication avoidance yields tangible benefits even at moderate scale as $s$ increases.

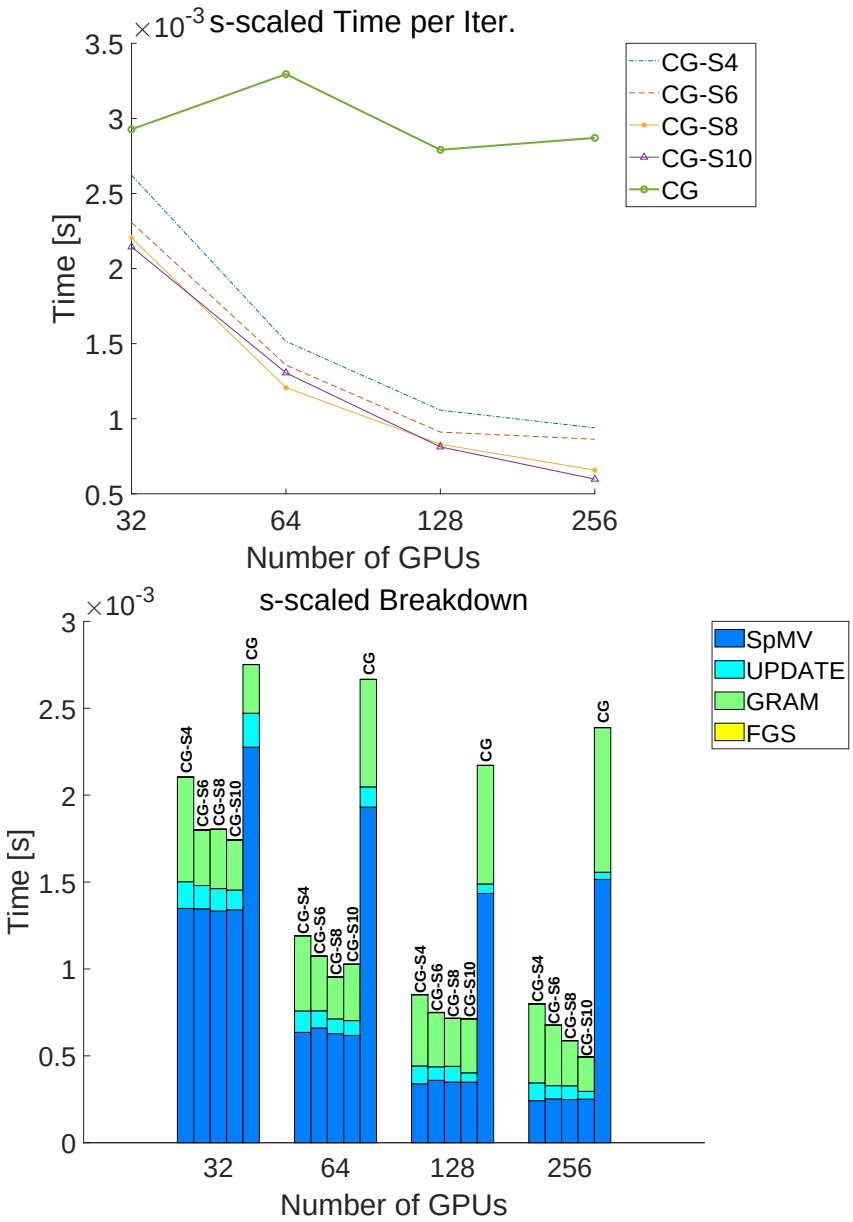


Figure 7: Strong scalability: time per iteration scaled by step size s (top) and related breakdown (bottom).

In agreement with the model, as $P$ grows the magnitude of $\Delta_{\text{strong}}$ increases with $s$, and the difference becomes more pronounced at larger scales. This trend highlights the increasing impact of global reductions as both $P$ and $s$ grow, confirming that communication-avoiding strategies are particularly effective in the large-scale regime.

Fixing the iteration count isolates system-level effects and shows that reducing the number of global reductions per iteration directly improves strong-scaling efficiency. When normalized by $s$, the per-iteration time of the $s$-step CG method decreases nearly monotonically with $P$ for larger $s$, indicating that the additional arithmetic work is effectively amortized by the reduction in communication latency.

The breakdown analysis in Figure 7 further shows that, as $P$ increases, global reductions associated with dot products account for an increasingly large fraction of the runtime in classical CG. The $s$-step formulation mitigates this cost substantially. SpMV remains the dominant kernel, while vector operations and reductions are significantly re-

duced in the $s$-step setting. The FGS Gram solve is negligible in these tests, representing under 1% of the per-iteration solve time even for the largest $s$ (Figure 7, bottom panel).

For completeness, Figure 8 reports the speedup of CG and the CG-S variants. While CG exhibits limited strong scalability, the CG-S variants scale increasingly better as $s$ grows, consistently with the reduced frequency of global communications. The only notable exception occurs at 512 GPUs, where the CG-S variant with $s = 8$ shows a performance drop that warrants further investigation.

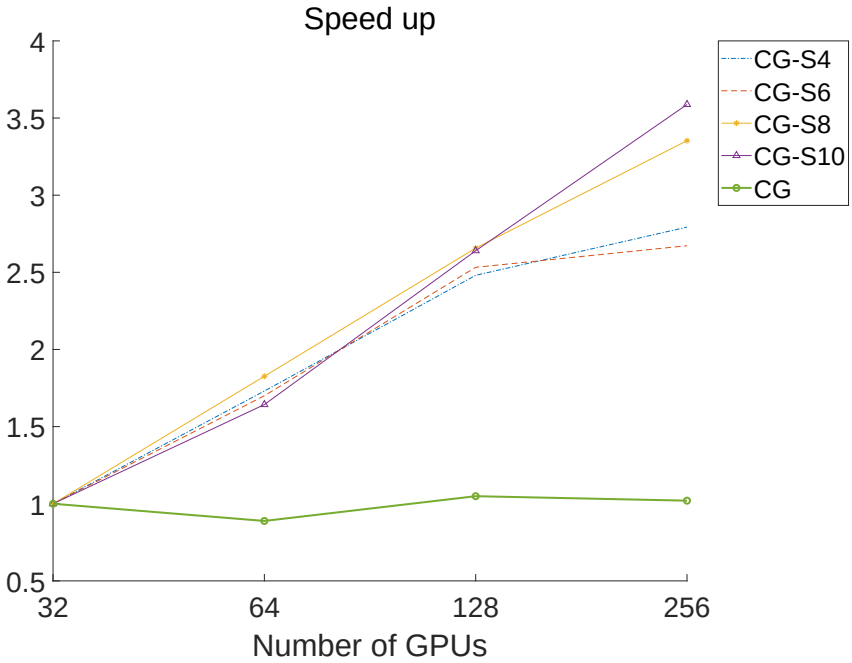


Figure 8: Strong scalability: Speed up.

## 6.2 Weak Scalability

In this section, we evaluate the weak scalability of the solver by increasing the number of DOFs proportionally to the number of GPUs, while keeping the local problem size fixed at $200^3$ DOFs per GPU. Experiments were performed on up to 512 GPUs of the Leonardo supercomputer, solving linear systems with more than 4 billion DOFs in total.

To assess algorithmic scalability and numerical robustness, we consider the preconditioned variant of PCG-S, employing the Algebraic MultiGrid (AMG) method implemented in `BootCMatchGX` and described in [1], configured with a W-cycle. As in the parametric study and previous experiments, the reduced Gram systems are solved using $\nu = 30$ iterations of the FGS method.

For all test cases, the solver is run with a relative residual tolerance $\text{tol} = 10^{-6}$ and a maximum of $\text{it}_{\max} = 1000$ iterations. Results are compared against the corresponding classical PCG method.

Figure 9 reports the weak-scaling behavior in terms of outer iterations (top) and total solve time (bottom).

The iteration count of PCG is consistently higher than that of the PCG-S variants, and the gap widens as the step size $s$ increases. This indicates that, as expected, the Chebyshev-based block construction improves the effectiveness of each outer iteration.

For fixed $s$, the iteration count remains relatively stable as the number of GPUs grows, with improved stability observed for larger $s$. This confirms that the $s$-step formulation

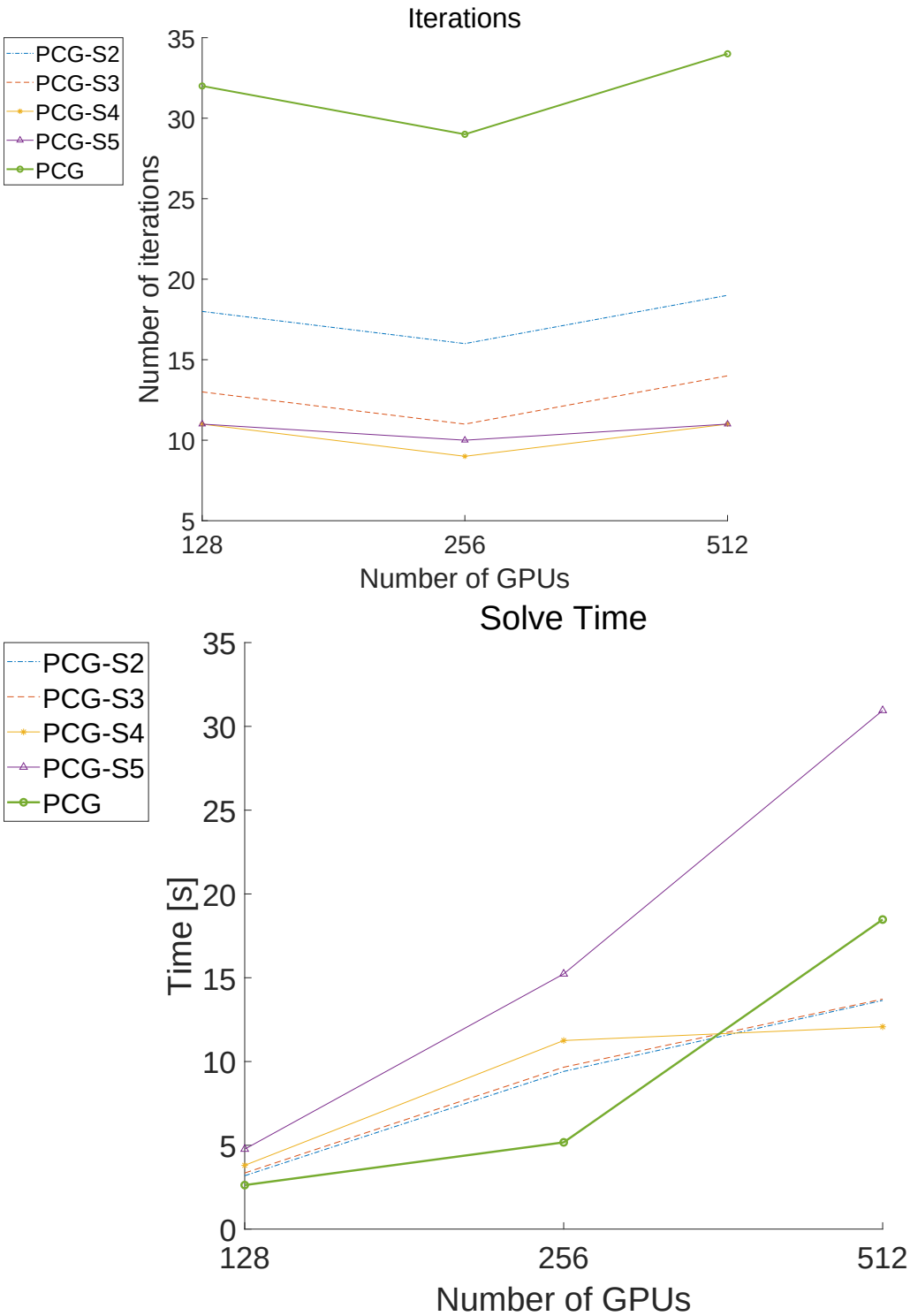


Figure 9: Weak scalability: number of iterations (top) and total solve time (bottom).

preserves robust convergence under weak scaling. Moreover, the Chebyshev basis combined with the AMG preconditioner remains stable across the tested scales, confirming that the spectral regularization induced by the preconditioner is compatible with the block polynomial construction.

In terms of total solve time, a clear effect emerges at 512 GPUs: for moderate step sizes ($s = 2, 3, 4$), the PCG-S solver outperforms PCG. In this regime, the reduction in outer iterations offsets the higher per-iteration cost of the $s$-step formulation, demonstrating that reduced communication can translate into tangible time-to-solution improvements

at scale.

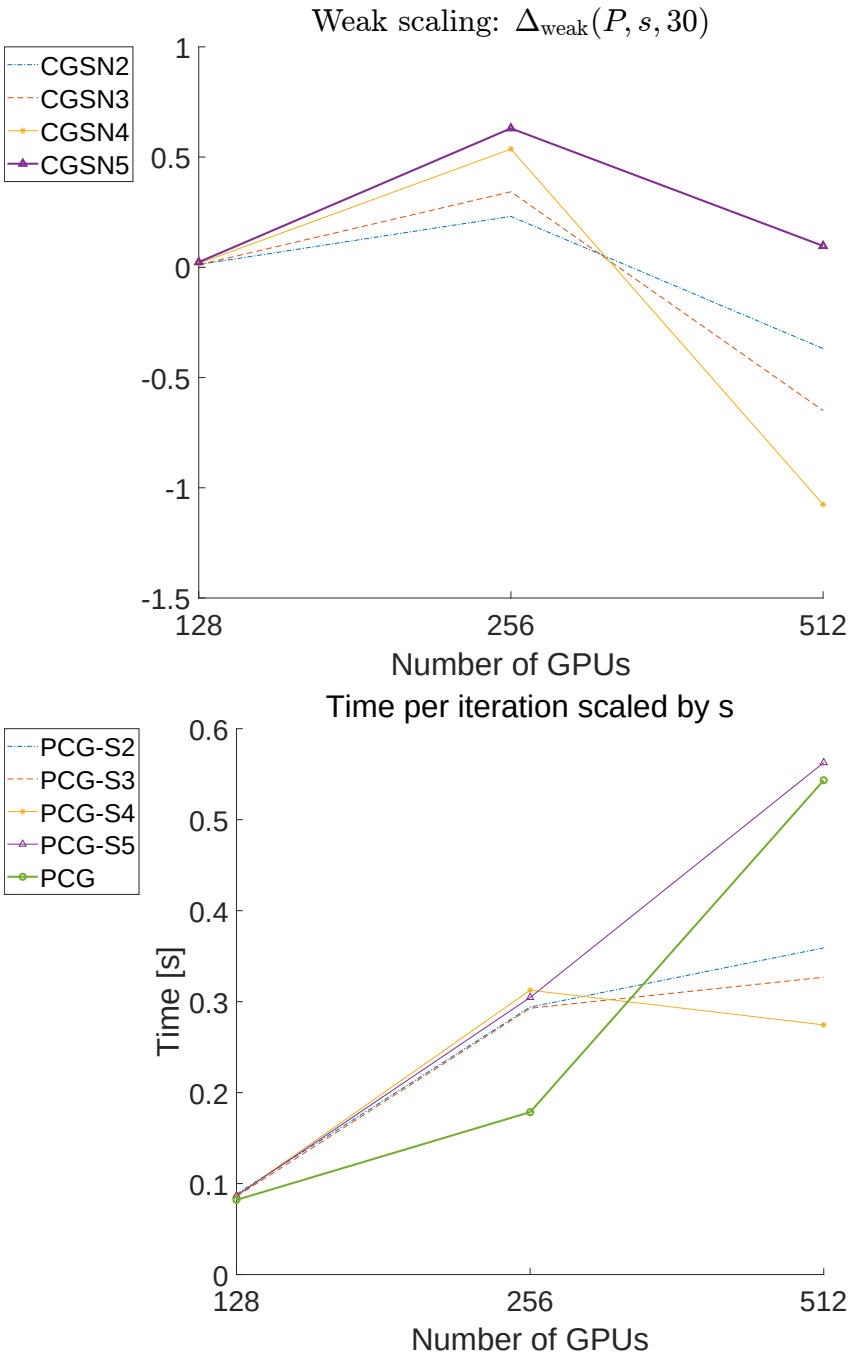


Figure 10: Weak-scaling behavior of $\Delta_{\text{weak}}(P, s, \nu = 30)$ (top) and time per iteration normalized by the step size $s$ (bottom).

Figure 10 (top) reports the weak-scaling indicator $\Delta_{\text{weak}}(P, s, \nu = 30)$. As the number of GPUs increases, the indicator decreases and becomes negative at 512 GPUs for $s = 2, 3,$ and 4. A negative value indicates that the $s$-step formulation outperforms PCG in terms of time-to-solution under weak scaling. This behavior is consistent with the performance model of Section 4.1, which predicts that communication savings become dominant at sufficiently large $P$.

The discrepancy observed for $s = 5$ at 512 GPUs is plausibly attributable to increased sensitivity to system noise and tail-latency effects in global collectives at extreme scale. A more detailed analysis at larger process counts would be required to fully characterize

this behavior.

The bottom panel of Figure 10 reports the scaled time per outer iteration, showing a trend consistent with the weak-scaling indicator in the top panel. For $s = 2, 3$, and 4, the scaled per-iteration time decreases at 512 GPUs, confirming that communication reduction effectively compensates for the additional local computation introduced by the $s$-step formulation. Combined with the reduced number of outer iterations observed in Figure 9, this explains the improved time-to-solution achieved by these configurations.

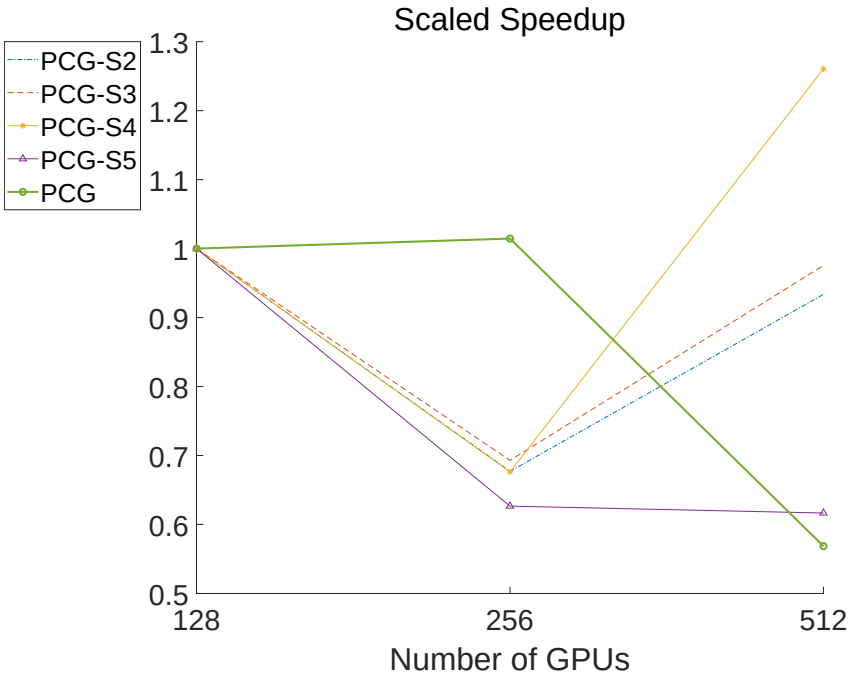


Figure 11: Weak scalability: scaled speedup.

Figure 11 reports the scaled speedup under weak scaling. At 512 GPUs, PCG exhibits a noticeable performance degradation, indicating that synchronization costs and collective latency effects increasingly limit scalability at extreme concurrency.

In contrast, the $s$-step variants with $s = 2, 3$, and 4 show an increasing scaled speedup as the number of GPUs grows. Among these, $s = 4$ achieves the best overall performance, providing the most favorable balance between communication reduction and additional local computation.

These results indicate that moderate step sizes offer the best trade-off at 512 GPUs. Verifying whether the theoretical model—which predicts increasing benefits for larger block sizes as $P$ grows— continues to hold beyond the tested regime will require experiments at larger scales.

Overall, the experiments demonstrate that the Chebyshev basis yields well-conditioned Krylov blocks, while the FGS solution of the Gram system remains numerically stable with a very negligible overhead in the tested regime, validating the design choice of combining these components.

Under weak scaling, the $s$-step formulation improves time-to-solution at 512 GPUs for moderate step sizes ($s = 2, 3, 4$), where the reduction in outer iterations compensates for the additional local computation. In this regime, $s = 4$ provides the most favorable balance between communication reduction and arithmetic overhead.

These findings suggest the existence of an optimal moderate step size in the explored range. At larger GPU counts, the interplay between communication and computation will remain the determining factor, and careful selection of $s$ will be essential to fully

exploit the advantages of the $s$-step approach.

# 7 Concluding Remarks and Future Work

We presented a scalable multi-GPU implementation of the s-step PCG method combining a Chebyshev-stabilized Krylov basis with an iterative FGS solver for the reduced Gram systems.

The experimental results indicate that the method exhibits satisfactory numerical robustness within the tested configurations, and that the proposed performance model reflects the main observed scalability trends. In strong scaling, the s-step variants tend to become competitive with, and in several cases faster than, classical CG as the number of GPUs increases, suggesting that synchronization costs play an increasingly relevant role at scale. In weak scaling with AMG preconditioning, reductions in time-to-solution are observed at 512 GPUs for moderate step sizes ($s = 2, 3, 4$), with $s = 4$ offering a favorable compromise between communication reduction and additional arithmetic cost in the explored regime. Convergence has been observed on problems exceeding 4 billion degrees of freedom.

For moderate values of $s$, the Chebyshev-based blocks appear to remain sufficiently well conditioned, and a fixed small number of FGS sweeps provides an adequate and inexpensive approximation of the Gram solves in the tested scenarios, without evidence of a significant performance penalty. For larger-scale settings, an adaptive Gram solver strategy based on the relative residual of the reduced system, allowing the inner accuracy to vary across outer iterations in accordance with inexact Krylov principles—could offer additional flexibility in balancing robustness and efficiency.

Further investigation at larger node counts and for larger step sizes is required to better characterize the method in more extreme regimes. Within the scales currently examined, the implementation appears to make effective use of modern GPU-accelerated architectures. Since communication is typically more energy-intensive than computation, reducing global synchronization and increasing computational locality may also have favorable implications for energy efficiency, although a dedicated study would be necessary to assess this aspect quantitatively.

Since robust preconditioning generally represents a dominant portion of the runtime, future work should also address the design of robust AMG-like strategies that preserve spectral regularization while minimizing synchronization overhead. Reducing communication within the preconditioner, increasing local computational density, and exploring adaptive precision mechanisms are key directions to further improve scalability and time-to-solution on GPU platforms.

Beyond the algorithmic and theoretical contributions, the work provides, to the best of our knowledge, the first available fully distributed multi-GPU implementation of preconditioned $s$-step CG at the scale reported here.

# Acknowledgments

We acknowledge Spoke 6 “Multiscale Modelling & Engineering Applications” of the Italian Research Center on High-Performance Computing, Big Data, and Quantum Computing (ICSC), funded by MUR-NextGenerationEU (NGEU), for awarding access to Leonardo at CINECA (Italy). We also acknowledge the EuroHPC Joint Undertaking

for awarding access to MareNostrum5 at BSC (Spain) under the EuroHPC Development Access call, which supported the computational experiments presented in this paper.

# References

[1] M. Bernaschi, A. Celestini, F. Vella, and P. D'Ambra. A Multi-GPU Aggregation-Based AMG Preconditioner for Iterative Linear Solvers. *IEEE Transactions on Parallel & Distributed Systems*, 34(08):2365–2376, 2023.

[2] A. Bouras and V. Frayssé. Inexact matrix-vector products in Krylov methods for solving linear systems. *SIAM J. Matrix Anal. Appl.*, 26(3):660–678, 2005.

[3] E. C. Carson. The adaptive $s$-step Conjugate Gradient method. *SIAM Journal on Scientific Computing*, 40(1):A297–A320, 2018.

[4] E. C. Carson, T. Gergelits, and I. Yamazaki. Mixed precision $s$-step Lanczos and Conjugate Gradient algorithms. *Numerical Linear Algebra with Applications*, 29(4):e2425, 2022.

[5] E. C. Carson, N. Knight, and J. Demmel. An efficient deflation technique for the Communication-Avoiding Conjugate Gradient method. *Electronic Transactions on Numerical Analysis*, 41:96–113, 2014.

[6] E. C. Carson, M. Rozložník, Z. Strakoš, P. Tichý, and M. Tůma. The numerical stability analysis of pipelined Conjugate Gradient methods: historical context and methodology. *SIAM Journal on Scientific Computing*, 40(5):A3549–A3580, 2018.

[7] A. Chronopoulos and C. Gear. On the efficient implementation of preconditioned s-step Conjugate Gradient methods on multiprocessors with memory hierarchy. *Parallel Computing*, 11(1):37–53, 1989.

[8] A. Chronopoulos and C. Gear. s-step iterative methods for symmetric linear systems. *J. Comput. Appl. Math.*, 25(2):153–168, 1989.

[9] S. Cools and W. Vanroose. The communication-hiding pipelined Conjugate Gradient method with deep pipelines. *SIAM Journal on Scientific Computing*, 2017.

[10] J. Cornelis, S. Cools, and W. Vanroose. Numerically stable recurrence relations for the communication-hiding pipelined Conjugate Gradient method. *IEEE Transactions on Parallel and Distributed Systems*, 30(11):2579–2593, 2019.

[11] P. D'Ambra, S. Filippone, and P. S. Vassilevski. BootCMatch: a software package for bootstrap AMG based on graph weighted matching. *ACM Transactions on Mathematical Software*, 44(4):39:1–39:25, 2018.

[12] J. Demmel, M. Hoemmen, M. Mohiyuddin, and K. Yelick. Avoiding communication in computing Krylov subspaces. *SIAM Journal on Scientific Computing*, 35(5):A1520–A1548, 2013.

[13] P. Ghysels and W. Vanroose. Hiding global synchronization latency in the preconditioned Conjugate Gradient algorithm. *Parallel Computing*, 40(7):224–238, 2014.

[14] L. Grigori, S. M. Moufawad, and F. Nataf. Enlarged Krylov subspace Conjugate Gradient methods for reducing communication. *SIAM Journal on Matrix Analysis and Applications*, 37(2):744–773, 2016.

[15] L. Grigori and O. Tissot. Scalable linear solvers based on enlarged Krylov subspaces with dynamic reduction of search directions. *SIAM Journal on Scientific Computing*, 41(5):C522–C547, 2019.

[16] M. Hoemmen. *Communication-Avoiding Krylov subspace methods*. PhD thesis, University of California, Berkeley, 2010.

[17] B. R. Lowery and J. Langou. Stability analysis of QR factorization in an oblique inner product, 2014.

[18] V. Mayer and W. N. Gansterer. Numerical properties and scalability of s-step preconditioned Conjugate Gradient methods. In *Proceedings of the International Conference for High Performance Computing, Networking, Storage, and Analysis (SC '25)*, New York, NY, USA, 2025. Association for Computing Machinery.

[19] V. Mayer and W. N. Gansterer. On combining pipelining and s-step concepts in preconditioned Conjugate Gradient methods. In *Proceedings of the SIAM Conference on Parallel Processing for Scientific Computing*. SIAM, 2026.

[20] B. Philippe and L. Reichel. On the generation of Krylov subspace bases. *Applied Numerical Mathematics*, 62(9):1171–1186, 2012.

[21] M. Rozloznik, J. Kopal, M. Tuma, and A. Smoktunowicz. Numerical stability of orthogonalization methods with a non-standard inner product. *BIT Numerical Mathematics*, 52:1035–1058, 2012.

[22] A. Ruhe. Numerical aspects of Gram-Schmidt orthogonalization of vectors. *Linear Algebra and its Applications*, 52:591–601, 1983.

[23] S. J. Thomas. A block algorithm for orthogonalization in elliptic norms. In *Lecture Notes in Computer Science*, volume 634, pages 379–385, 1992.

[24] S. J. Thomas, E. C. Carson, M. Rozložník, A. Carr, and K. Świrydowicz. Iterated Gauss–Seidel GMRES. *SIAM Journal on Scientific Computing*, 46(2):S254–S279, 2024.

[25] S. J. Thomas and P. D'Ambra. Inexact Gauss–Seidel coarse solvers for AMG and $s$-step CG. arXiv preprint arXiv:2512.09642, 2025. https://arxiv.org/abs/2512.09642.

[26] S. J. Thomas and R. V. M. Zahar. Efficient orthogonalization in the M-norm. *Congressus Numerantium*, 80:23–23, 1991.

[27] S. J. Thomas and R. V. M. Zahar. An analysis of orthogonalization in elliptic norms. *Congressus Numerantium*, 86:193–193, 1992.

[28] M. Tiwari and S. Vadhiyar. Pipelined preconditioned s-step Conjugate Gradient methods for distributed memory systems. In *2021 IEEE International Conference on Cluster Computing (CLUSTER)*, pages 215–225, 2021.

[29] M. Tiwari and S. Vadhiyar. Pipelined preconditioned Conjugate Gradient methods for real and complex linear systems for distributed memory architectures. *Journal of Parallel and Distributed Computing*, 163:147–155, 2022.

[30] J. van den Eshof and G. L. G. Sleijpen. Inexact Krylov subspace methods for linear systems. *SIAM Journal on Matrix Analysis and Applications*, 26(1):125–153, 2004.